SIMON FRASER UNIVERSITY

Undergraduate Thesis

Current Loop Off-Axis Field Approximations

By
Daniel Carleton

Undergraduate thesis submitted in partial fulfillment of the
requirements for the Degree of
Bachelor of Applied Science (Honours)

In the
School of Engineering Science
Faculty of Applied Sciences

SIMON FRASER UNIVERSITY
Fall 2022

APPROVAL

Name: Daniel Carleton

Degree: Bachelor of Applied Science Honours

Title of Thesis: Current Loop Off-Axis Field Approximations

Dr. Michael Sjoerdsma, P.Eng.
Acting Director, School of Engineering Science

Examining Committee:

Dr. Glenn Chapman, Academic/Technical Supervisor
Professor, School of Engineering Science

Dr. Marinko Sarunic, P.Eng
Professor, School of Engineering Science

Dr. Steve Dodge
Professor, Department of Physics

Date Approved: April 18, 2023

Declaration of Committee

Name:	**Daniel Carleton**
Degree:	**Bachelor of Applied Science**
Title:	**Undergraduate Thesis Proposal**
Committee:	**P.Eng, Dr. Glenn Chapman** Academic and Technical Supervisor Professor, School of Engineering Science
	P.Eng, Dr. Marinko Sarunic Committee Member Professor, School of Engineering Science
	Dr. Steven Dodge Committee Member Associate Professor, Department of Physics

Abstract

The idealized thin current loop is the foundation for cylindrically symmetric applied coil magnetics. The field equations along the coil axis are easy to solve both numerically and analytically, however, the equations for the fields away from the axis are significantly more complex. The off-axis field equation can be derived from Biot-Savart law and the exact solution involves the difference of elliptical integrals of the first and second kind which make the field difficult to visualize and numerically expensive to calculate.

We have derived a new set of approximations to the current loop equations using a binomial expansion of the elliptical integrals. The resulting terms of the expansion are fitted to minimize the maximum relative error of the approximation over all space. The resulting approximation is exactly correct along the loop axis, at infinity, and it is highly accurate with a low computational cost everywhere else. This approximation is broken down into 5 orders of increasing accuracy and computational cost for the radial and axial components of the magnetic field. For the radial field, the first and second order maximum relative errors are approximately 2.5×10^{-2} and 2.9×10^{-4} respectively. The higher ordered radial approximations add additional corrective terms with the third, fourth, and fifth ordered approximations having a maximum relative error of 1.8×10^{-5}, 4.3×10^{-6}, and 4.9×10^{-7} respectively.

Similarly, the axial approximations are highly accurate between the loop and coil axis (h<a) as well as on the loop plane. However, off the plane it diverges as we approach the location where the axial field changes polarity. This is due to the slight difference in location where the axial field changes polarity given by the exact equations and approximations. Therefore, when calculating the relative error of the axial field at the exact polarity changing location, the approximation's axial is slightly non-zero. This leads to a significantly large relative near these locations although the absolute error is negligible. Outside of the polarity reversing locations, the axial relative error decays to zero. Both the axial and radial approximations are computationally simple algebraic functions. Additionally, 3D relative error plots for the magnetic field inside and outside of the loop are presented and discussed for all orders of approximation to visualize their behaviour.

We have applied these approximations to a common engineering system, the Helmholtz coil, which is a pair of identical coils separated by a distance equal to their radii. As our approximation is exactly correct along the axis, deriving the Helmholtz coil spacing from the approximation is computationally simple. Furthermore, we have shown that the third order approximation offers the highest accuracy for a nearly negligible computational cost when compared to second order. Using the first order approximation, we have derived a simple algorithm allows engineers to quickly calculate what coil radius is required to produce a sufficiently uniform field for a known volume. This algorithm has also been expanded to the second and third ordered approximations if an extremely high accuracy is required at the expense of a small increase in computational cost.

Acknowledgements

I would like to acknowledge and give my warmest thanks to my supervisor, Dr. Glenn Chapman, who made this thesis possible. His guidance and advice helped me throughout the many stages of my USRA and now my undergraduate thesis. I would also like to thank my committee members, Dr. Steve Dodge and Dr. Marinko Sarunic, for participating in my defense and for their feedback.

Table of Contents

List of Tables

List of Figures

List of Acronyms

Term	Definition
SFU	Simon Fraser University
FEA	Finite Element Analysis

Chapter 1. Introduction

1.1 Background

Electromagnetism is one of the fundamental forces of our universe and has many applications throughout modern technology. Electromagnetic fields are harnessed for modern technology in a wide variety of areas including electric motors, audio equipment, and MRI machines. All these applications must be designed to produce the correct shape of magnetic field, but accurately simulating these fields is difficult and computationally expensive. One of the fundamental devices in undergraduate physics classes we learn to derive the magnetic field generated by a thin current loop using Biot-Savart law.

Biot-Savart law was discovered in 1802 and allowed for analytic calculations to express the magnetic field that results from constant electric current in a wire. This equation easily calculates the magnetic field generated on the axis of a current loop due to the symmetry there, but to calculate the off axis magnetic field, the equations become significantly more complex. Dating back to the 1900's, complete equations to yield off-axis solutions were derived using the elliptical integrals of the first and second kind but those are highly complex to calculate with high accuracy. However, with the power of modern computing, these equations are either often solved numerically using Finite Element Analysis (FEA) or direct numerical evaluation using a numerical processing library such as Python's scientific computing library SciPy thanks to the massive advances in computational power since the late 1900's. Due to these advances, there have been few attempts to re-examine these equations and look for better approximations. The much simpler approximations derived for this thesis are computationally less expensive, highly accurate, and may be used to quickly solve complex magnetic systems significantly faster than modern day FEA.

The most common analytic off-axis field equations contain for the thin current loop contain elliptical integrals, they are hard to manipulate, difficult to project how they change with position and computationally expensive to evaluate. Although with a fundamental understanding of magnetism, one knows how the magnetic field of a thin current loop behaves, but this behaviour is not obvious from these equations alone. The simple behaviour of the magnetic field of the current loop is hidden behind a complex equation that masks its simple behaviour.

Despite these challenges with the exact analytic solutions, I believe we have found a computationally simple approximation that fulfills these drawbacks. These approximations use a binomial series expansion on the elliptical integrals to create approximate series solutions. This series can be simplified and approximated to yield an amazingly simple equation with analytical solutions, high accuracy, and computationally low cost. Additionally, the approximated equation is easy to understand without intensive calculations.

Consider a thin circular current loop as shown below in Fig. 1 that is concentric and co-planar with the x-y plane and we want to evaluate its magnetic field at a point P. We can derive the equation for this system from Biot-Savart law in cylindrical coordinates with the following parameters.

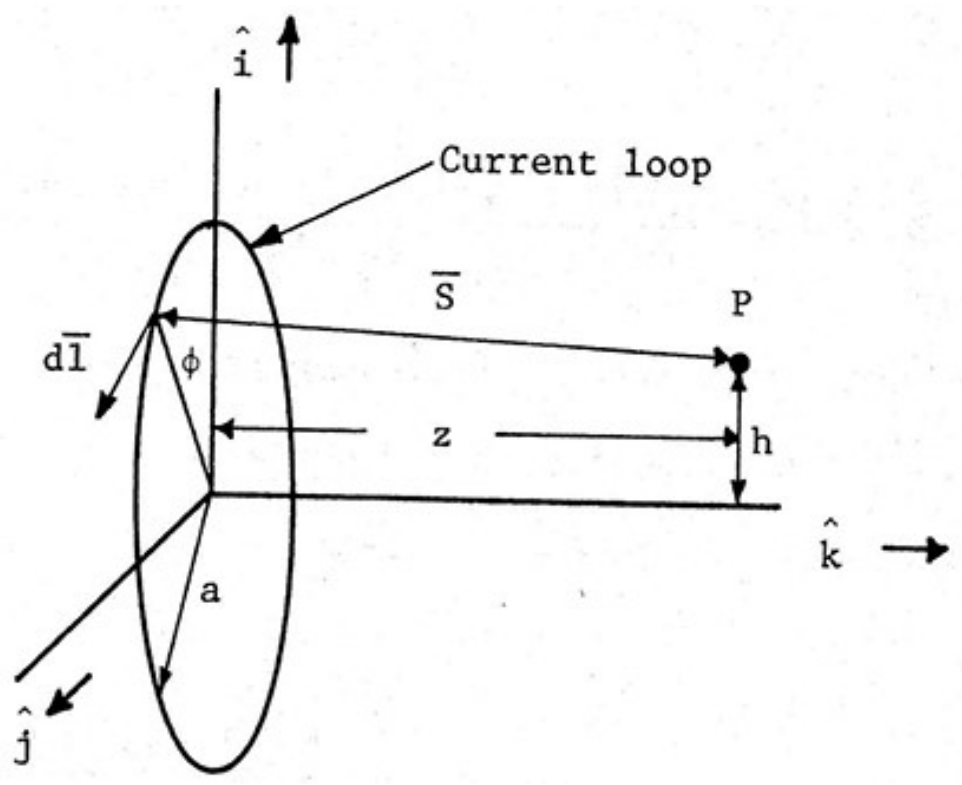

Fig. 1. Magnetic field due to thin current loop at point P [1].

a	=	Loop radius	ϕ	=	Angular coordinate of P
h	=	Radial coordinate of P	I	=	Loop current
z	=	Axial coordinate of P			

This results in the following equation for the off-axis magnetic field in the radial and axial directions labelled B_r and B_a respectively [2].

$$B_r = \frac{\mu_0 I}{2\pi}\int_0^{\pi} \frac{za\,cos(\phi)\,d\phi}{\left(h^2 + a^2 + z^2 - 2ha\,cos(\phi)\right)^{3/2}} \quad (1)$$

$$B_z = \frac{\mu_0 I}{2\pi}\int_0^{\pi} \frac{\left(a^2 - ha\,cos(\phi)\right)d\phi}{\left(h^2 + a^2 + z^2 - 2ha\,cos(\phi)\right)^{3/2}} \quad (2)$$

The most common representation of the thin current loop equations are elliptical integrals of the first kind E(k') and second kind K(k') in cylindrical coordinates, as shown in Eqs. 3 and 4. The integrands of these equations are the elliptical integrals and are analytically complex as well as computationally costly. Additionally, the elliptical integrals make it difficult visualize the system's behaviour from the equations alone. Despite these challenges, there are efficient approximate solutions [3].

$$B_r = \frac{\mu_0 I}{2\pi} \frac{z}{h[(h+a)^2+z^2]^{1/2}} \left[-K(k') + \frac{h^2+a^2+z^2}{(a-h)^2+z^2} E(k') \right] \quad (3)$$

$$B_z = \frac{\mu_0 I}{2\pi} \frac{1}{h[(h+a)^2+z^2]^{1/2}} \left[K(k') + \frac{h^2-a^2-z^2}{(a-h)^2+z^2} E(k') \right] \quad (4)$$

$$k' = \left[\frac{4ah}{(h+a)^2+z^2} \right]^{1/2} \quad (5)$$

1.2 Problem

The complex analytic solutions for the thin current loop make it exceedingly difficult to create computational quick and accurate simulations when designing a magnetic system. These equations have simple analytic solutions on the axis of the coil, but the off-axis equations are highly complex and difficult to accurately evaluate. One could use a lookup table to evaluate the elliptical integrals, but this method is tedious and inaccurate [4]. Additionally, since the analytic equations contain the difference of elliptical integrals of the first and second kind, a high degree of numerical accuracy is required to approximate these equations. However, various infinite series solutions do exist which provide accurate solutions to these elliptical integrals, they are still highly complex requiring a significant number of terms to reach sufficient accuracy [5, 6].

One method is to use a partial power series decomposition of Laplace's equation about the loop axis, for which the field is angularly symmetric. Then the series coefficients of the expansion are found by taking the derivatives of the field along this axis. This method approximates the field to within 0.1% from the elliptical integral equations, but only out to approximately 70% of the radius of the loop [6]. Another method uses Fourier integral properties to expand the elliptical equations to yield a series form. This process yields an infinite series approximation that also requires evaluating an infinite series of double derivatives of its own series solutions. This method, for the highest order derivatives yields an error below 1% for a point P located less than 0.8 loop radii from the loop axis [5].

Alternatively, this system can be solved with Finite Element Analysis (FEA). FEA works by breaking down the loop into many discrete straight regions (transforming the loop into an n-sided polygon) and calculating the magnetic field vector components from each region at a every point in the region of interest. This is process is straightforward but requires many calculations as you must iterate through each region of the loop and each node in the spatial region and higher accuracy requires high numbers of segments. However, with the rise of computational power, finite element analysis (FEA) has become the most common way to model these systems. There are commercially available programs FEA programs, such as Ansys Maxwell, that can be used to model off axis magnetic systems quickly and accurately [7]. However, improving the accuracy of FEA requires an increase in the number of finite elements of your system leading to an increase in computational cost and complexity.

Our new approximate solutions provide a computationally simple and highly accurate approximation to these elliptical integrals with a new series solution. These approximations are exact along the loop axis and at great distances from the loop and have very low relative error across all space. These approximations are simple algebraic equations and do not involve any calculus. This also suggests this approximation is very computationally efficient compared to current methods. And perhaps most importantly, the behaviour of the field is easy to visualize from the equations alone.

1.3 Scope

Dr. Chapman originally discovered this solution type in the series form during his master's thesis in 1975. Later he then derived the first, second, and third order approximations between 1999 and 2002 which are shown in Chapter 2. Mr. Sahota during an NSERC USRA performed the curve fitting of the coefficients of the approximations as a USRA student of Dr. Chapman in 2010. Mr. Sahota and Dr. Chapman showed that these approximations had low maximum relative error when compared to the elliptical equations. However, these plots were only 2 dimensional and did not fully explore the approximation in 3D space.

My work began in 2021 as a USRA student for Dr. Chapman, where I was tasked with exploring these approximations across all of 3D space. My major task was to create a spatially 3D map of the relative error of the new approximations comparing them to the elliptical integral equations. My first step was to create my simulation and ensure that its results matched the previous work done by Dr. Chapman and Mr. Sahota.

My simulations were necessary to demonstrate the accuracy of these approximations. Through my work during my USRA, Dr. Chapman and I published a conference article to the Joint MMM-Intermag Conference in February 2022 where our work was accepted for a full journal article which was published in in August 2022 [8, 1]. My work has expanded to include applying these approximations to Helmholtz coil applications.

1.4 Thesis Explorations

My simulations calculated the magnetic field using the elliptical equations and the new approximations and found their relative and absolute error at every point in space for the radial and axial magnetic field vectors as well as their magnitude. The field solutions for the new approximations utilized the equations derived by Dr. Chapman and the numerical fitting of the coefficients derived by Mr. Sahota. Additionally, I could check the validity of my simulations by comparing my results to those previously achieved. My work included rederiving the approximations, and then creating a script in Maple for each order of approximation to perform the relative and absolute error analysis using Maple's built in elliptical integral equation library. An important point is that this work explained several anomalous results that had arisen in the earlier work in 3D space giving us the confidence that the approximations were working correctly. At the end of my USRA, Dr. Chapman and my research was accepted into the joint MMM Intermag 2021 conference (largest conference in the field) and presented remotely, due to covid pandemic, at the conference in Jan 2022 in New Orleans [1]. The conference selected the paper for the expanded full journal version from that conference section and after peer review was published in electronically in

February 2022 while the printed version was released in the August 2022 issue of the IEEE Transactions on Magnetics journal [8].

1.5 Organization

The purpose of this work was to demonstrate the simplicity of these new approximations and confirm their accuracy through numerical simulations. This thesis will be broken down into 4 chapters. Chapter 1 of this thesis will introduce the off-axis field equations for a simple current loop derived from Biot-Savart Law. Then discuss the shortcomings and problems in solving these equations analytically and approximately with common methods and why these equations are important.

Chapter 2 outlines the analytic derivations of the new approximations, the simulation methods, and finally showcases the results of the first order approximation. Highlighting what we discovered through and a discussion on the interesting behaviour. Chapter 3 expands on chapter 2 to include the simulations for higher order approximations from second to fifth order.

Chapter 4 will show how the Helmholtz coil spacing can be rederived with these equations and show that our simple approximations provide a new equation to find the volume within a Helmholtz coil in which the magnetic field deviates by fewer than a specific percent.

Chapter 2. Derivations

The methods in this thesis are building upon previous research of Dr. Glenn Chapman, where he had derived a new series approximation to the current loop equations that may have some advantages over current approximations between 1999 and 2002. The denominator of the loop equations was modified so that the denominator of the integrand is always between 0 and 1 Therefore, we will get a converging infinite series solution with the binomial expansion. Starting from the elliptical integral equations derived from Biot-Savart Law, we see that the denominator is always less or equal to 1 or more explicitly.

$$\frac{2\mathrm{ha}\cos\phi}{h^2+a^2+z^2} \leq 1 \tag{6}$$

$$B_r = \frac{\mu_0 I}{2\pi}\frac{1}{(h^2+a^2+z^2)^{(3/2)}}\int_0^{\pi}\frac{za\cos(\phi)\,d\phi}{\left(1-\frac{2ha\cos(\phi)}{h^2+a^2+z^2}\right)^{(3/2)}} \tag{7}$$

$$B_z = \frac{\mu_0 I}{2\pi}\frac{a}{(h^2+a^2+z^2)^{(3/2)}}\int_0^{\pi}\frac{(a-h\cos(\phi))\,d\phi}{\left(1-\frac{2ha\cos(\phi)}{h^2+a^2+z^2}\right)^{(3/2)}} \tag{8}$$

2.1 Radial Field Approximation

Applying a binomial expansion to the denominator and expanding terms by term yields an infinite series of fractional factorials. Expanding each fractional factorial into its corresponding factorial/double factorial and simplifying can be converted back to a much simpler infinite series of integer factorials.

$$\left(1-\frac{2\mathrm{hacos}(\phi)}{h^2+a^2+z^2}\right)^{\frac{-3}{2}} = \sum_{n=0}^{\infty}\binom{n+\frac{1}{2}}{n}\left[\frac{2ha\cos\phi}{h^2+a^2+z^2}\right]^n = \sum_{n=0}^{\infty}\frac{(2n+1)!!}{2^n n!}\left[\frac{2ha\cos\phi}{h^2+a^2+z^2}\right]^n \tag{9}$$

Where the double factorial is defined as the following.

$$(2n+1)!! = 1\cdot 3\cdot 5\cdot\ldots\cdot(2n+1) \tag{10}$$

Substituting back into the elliptical integral equations yields the following.

$$B_r = \frac{\mu_0 I}{2\pi}\frac{za}{(h^2+a^2+z^2)^{\frac{3}{2}}}\sum_{n=0}^{\infty}\left[\frac{(2n+1)!!}{2^n n!}\left(\frac{2ha}{h^2+a^2+z^2}\right)^n\int_0^{\pi}(\cos\phi)^{n+1}\,d\phi\right] \tag{11}$$

Integrating the cosine term is the final step before evaluating the series, which we rely on the following relationship [3].

$$\int_0^{\pi} (\cos\phi)^{2k}\, d\phi = \pi \frac{(2k-1)!!}{2^k\, k!} \qquad (12)$$

We can appropriately shift the summation bounds to utilize this relationship, simplifying, and shifting the bounds back yields the following series equation.

$$B_r = \frac{\mu_0 I}{4} \frac{a^2 z h}{(h^2+a^2+z^2)^{5/2}} \sum_{n=0}^{\infty} \left[\frac{(4n+3)!!}{(n+1)\,(n!)^2\, 4^{2n}} W^n \right] \qquad (13)$$

Where we introduce a new term W, called the scaling factor, which is bound between 0 and 1 over all space.

$$W = \frac{4h^2 a^2}{\left(h^2+a^2+z^2\right)^2} \qquad (14)$$

We now have an infinite series that rapidly converges when W is small but converges slowly when W approaches one. We can also show that the coefficient of factorials of the W term rapidly approaches a constant value. First, we apply using Stirling's approximation to evaluate the factorials.

$$k! \approx \sqrt{2\pi k}\left(\frac{k}{e}\right)^k \left[1+\frac{1}{12k}\right] \qquad (15)$$

$$k!! \approx \sqrt{2k}\left(\frac{k}{e}\right)^{\frac{k}{2}} \qquad (16)$$

Applying Stirling's approximation to our factorial series and evaluating the limit as $n \to \infty$, gives the following solution.

$$\lim_{n\to\infty} \left[\frac{(4n+3)!!}{(n+1)\,(n!)^2\, 4^{2n}} \right] = \lim_{n\to\infty} \left[\frac{4n+3}{e} \right]^{\frac{4n+3}{2}} \frac{\sqrt{2(4n+3)}}{2\pi n\,(n+1)\,4^{2n}} \left(\frac{e}{n}\right)^{2n} \left(\frac{12n}{12n+1}\right)^2 \to \frac{8\sqrt{2}}{\pi} \qquad (17)$$

We note that in this series that the n=0 term is exactly equal to 3 and if the term in Eq 14, is approximately constant for the n>0 terms. With these considerations, we have the following equation.

$$B_r \approx \frac{\mu_0 I}{4} \frac{a^2 z h}{(h^2+a^2+z^2)^{\frac{5}{2}}} \left[3 + \frac{8\sqrt{2}}{\pi} \sum_{n=1}^{\infty} W^n \right] \qquad (18)$$

The infinite series is a converging power series, and if substitute a variable to replace the term inside the square brackets we arrive at the final form of our first order radial field approximation.

$$B_r \approx \frac{\mu_0 I}{4} \frac{a^2 z h}{(h^2+a^2+z^2)^{\frac{5}{2}}} A_R \qquad A_R = 3 + A_{R1}\left(\frac{W}{1-W}\right) \qquad A_{R1} = \frac{8\sqrt{2}}{\pi} \qquad (19)$$

From the approximation term A_R and noting that far from the loop and along the loop axis $W \to 0$, we see that that $A_R \to 3$. This simplifies our equation significantly in these regions and makes the behaviour of the magnetic field easy to visualize from the approximations.

Our first order radial field approximation is now a simple algebraic equation where the A_{R1} term represents 1 degree of freedom. While we analytically solved for its value, we can further improve the accuracy by curve fitting the coefficient to improve its accuracy. Numerically fitting these coefficients was completed by Mr. Sahota and Dr. Chapman in 2010 for the first through fifth order approximations.

2.2 Simulation Methods

The accuracy of these approximations was explored using a lattice of evenly spaced points which the axial and radial magnetic field was computed using Maple and their built-in elliptical functions. The lattice was linearly spaced and bounded out to ±10 loop radii. Due to the angular symmetry of the magnetic field, we only evaluated in the axial and radial directions (h,z dependent). Therefore, each lattice point has coordinates (h_i, z_j) at which we can evaluating the relative difference in the axial and radial magnetic field between the analytic elliptical equations and our new approximation.

$$\frac{B_{approx}(h_i, z_j) - B_{elliptical}(h_i, z_j)}{B_{elliptical}(h_I, z_j)} \quad (20)$$

My first goal was to recreate Mr. Sahota's radial field 2D plot as a function of W and a plot of the axial field in the loop plane (z=0). This was a great resource to confirm my algorithm before expanding the work into the 3D spatial plots. This also demonstrated the need for the higher precision of the curve fitting when minimizing the relative error. For the higher ordered approximations (3rd to 5th), a precision of 24 decimal places was used.

Maple was used for these simulations due to the convenience of having a predefined function for the elliptical integrals which we are relying on to evaluate the accuracy of our approximation. To evaluate the accuracy of the approximation, we plotted the relative error of the radial and axial components of the field as well as the magnitude. However, it had a few limitations when creating surface contours for the relative error. Namely, that creating a surface contour with a grid was not possible without significantly altering my current algorithm. To overcome this, the spacing on the grid was significantly reduced to effectively make a smooth surface with a color gradient represented on the z-axis to improve legibility. The axis labels represent the distance from the origin, positioned at the center of the current loop, in terms of the number of loop radii.

Additionally, when solving for the radial and axial fields there are a few important regions where the equations exhibit strange behaviour. Firstly, the axial magnetic field approaches infinity at the loop (h=a, z=0). This singularity occurs mathematically from the Elliptical field equations, which since we are examining the field due to a thing coil, this effectively occurs as we are solving or the field at a point. Secondly, for small h, the radial elliptical field equations are unstable and require an enormous amount of precision to accurately evaluate the difference of two elliptical integrals. For example, at the center of

the loop (z=h=0), the magnetic field should be entirely in the axial direction, however with a precision of 24 decimal places, we get a relatively small, but non-zero radial field. This error in the field drops off as we move axially outward from this location along the coil axis. Evaluating the field along the coil axis for small z (fixed h=0) results in the following field solutions shown in

z	0	0.0001a	0.001a	0.01a	0.1a
Radial Field (T)	undefined	undefined	undefined	undefined	undefined
Axial Field (T)	undefined	6.283×10^{-7}	6.283×10^{-7}	6.282×10^{-7}	6.190×10^{-7}

TABLE I. Elliptical field solutions using Maple's elliptical function solver for h=0 and small z.

We see that at the exact centre of the coil, the radial and axial components of the field are actually undefined when using the elliptical solution. This behaviour is unexpected, as we expect the axial field to be the strongest (but finite) at the centre of the coil and the radial field to be zero along the coil axis. The undefined elements are the returned value from Maple's elliptical field solutions and represent a singularity at that location. In the elliptical equations (Eqs. 3 and 4), k' is zero when h=0 (see Eq. 5) and in the radial field equation (Eq. 3) there is a factor of z/h while the axial field equation (Eq. 4) has a factor of 1/h. These factors combined with the elliptical solutions for near zero h (the axis) and z values lead to computational difficulties even when retaining 20 decimal places. This is a known issue with the elliptical functions, and one must use these functions carefully to obtain accurate solutions along the coil axis [9]. R.A Schill even states that "For the on-axis limiting solution, it was observed that the radial component of the magnetic field as developed by others required careful handling of the coefficients of the elliptic functions in order to demonstrate that the field vanishes" [9]. This shows that these equations can be difficult to work with and require some expertise, particularly with the radial component along the coil axis where the parameter of the elliptical integrals k' (see Eq. 5) becomes singular (as h=z=0) which results in singular values of the field shown in TABLE I. We are relying on the accuracy of Male's elliptical solutions, and they exhibit strange behaviour along the coil axis. However, a small deviation from the coil axis corrects these singularities in the elliptical solutions, therefore, to work around this issue, the simulations lower bound will start at 0.001a for both the radial (h) and axial (z) coordinates. However, as this thesis will show, the on-axis field equations from our approximation are exactly correct and do not require any special handing or limitations on spatial parameters. Most importantly the approximations in this thesis do not have the same issues. For example, the radial field approximation (Eq. 19) has a factor of h multiplying a function, so it inherently goes to zero when h=0 at the axis.

2.3 Radial Field Simulation

The first step in simulating the field was to numerically fit the coefficient to achieve the highest possible accuracy for the approximation. This corrects for any error when we assumed that the coefficient was constant for k>0. With only 1 degree of freedom, curve fitting the approximation has minimal effect on the approximation's accuracy. Mr. Sahota's work explored two options; the first option was to fit the coefficient so that the approximation is exactly correct at W=1. Remembering that the approximation is already exactly correct at W=0, so now our approximation is exactly correct along the loop axis and at the loop itself, W=0 and W=1 respectively. The second option was to fit the coefficient to minimize the maximum relative error which nearly halves the maximum relative error. Using Dr. Chapman's coefficients

for both methods result in the following plots in W space shown in Fig. 2 and Fig. 3. Fig.3 shows a fit where we use the A_{R1} value of equation (16), which yields a zero-error fit both at the axis and the current loop, which is useful for several applications. However, Hasting's showed that for these types of approximations the minimum error occurs when the negative and positive peaks of the relative error are equal in magnitude [9]. This is done in Fig. 2 by slightly changing the A_{R1} to 3.50561668537724 (found by numerical minimization). When you do that, the worst error is cut nearly in half, at the cost of having a small fractional error at the loop where the field strength goes to infinity by Eq. 19.

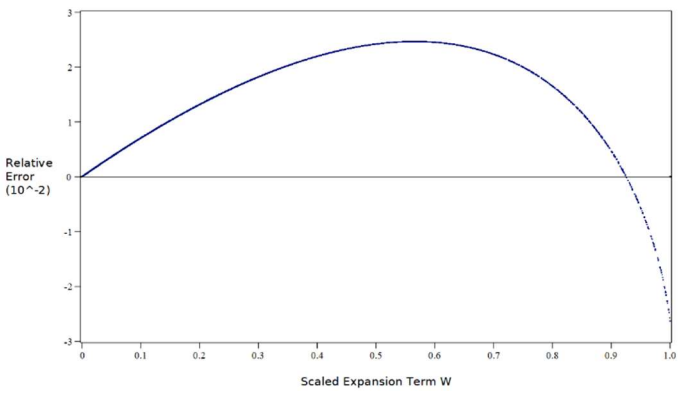

Fig. 2. First order relative error for the radial field in W space with minimized maximum relative error.
$A_{r1} = 3.50561668537724.$

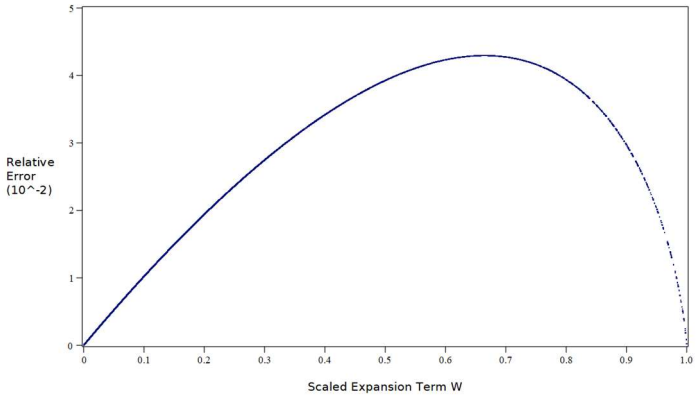

Fig. 3 First order relative error for the radial field in W space with two fixed endpoints.
$A_{r1} = 3.60126526462843.$

These plots in W space highlight the effectiveness of not only the approximation, but also the method used to fit the coefficients. For the remaining discussion of first order plots, we will use the better approximation where we minimized the maximum relative error. For this choice, the radial approximation is accurate to two significant figures over all space. However, it is hard to extrapolate the behaviour of the approximation in the spatial domain from W space. As such, there was room to expand this work across 3D space to completely visualize the behaviour of these approximations. Following the simulation methods, we created the following plot in Fig. 4 to visualize the relative error in 3D space.

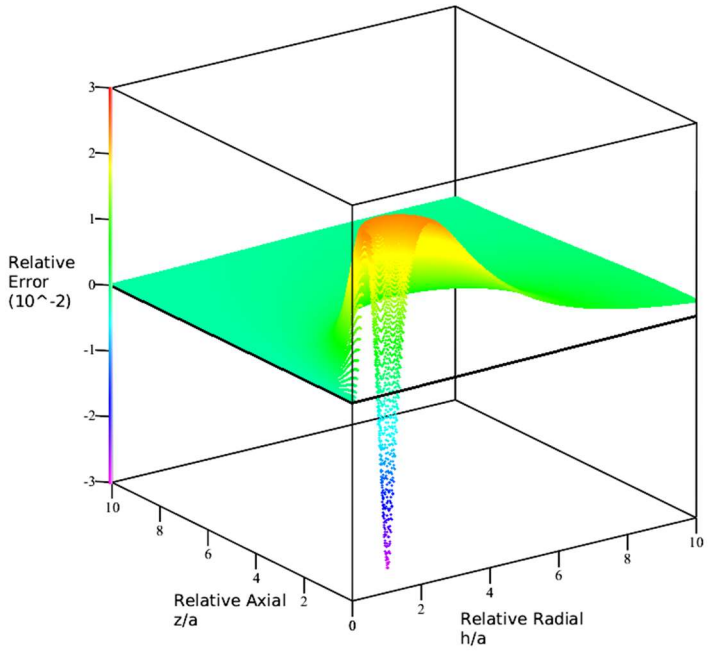

Fig. 4 First order relative error for the radial field approximation.

The radial relative error plot is nicely bounded and is exactly correct along the loop axis and far from the loop with a maximum relative error of 2.466×10^{-2} or 2.466%. This was somewhat hidden was W is equal to zero both along the loop axis and at great distances from the loop. Notably we see that the relative error is highest for small z, close to the loop, and is minimal as we move away from the loop regardless of how far we move radially from the loop.

2.4 Axial Field Approximation

We can perform the same methodology for the axial field equation, using the same binomial expansion in Eq 6.

$$B_z = \frac{\mu_0 I}{2\pi} \frac{a}{(h^2+a^2+z^2)^{\frac{3}{2}}} \sum_{n=0}^{\infty} \left[\frac{(2n+1)!!}{2^n n!} \left(\frac{2ha}{h^2+a^2+z^2} \right)^n \int_0^{\pi} (a - h\,cos\phi)(\cos\phi)^n \, d\phi \right] \quad (21)$$

We can expand the summation into the difference of two summations, which can then be manipulated in the same manner as for the radial derivation using the same relationship given in Eq 16 yields the following result.

$$B_z = \frac{\mu_0 I}{4(h^2+a^2+z^2)^{\frac{1}{2}}} \sum_{n=0}^{\infty} \left[\frac{(4n+1)!!}{4^{2n}(n!)^2} \frac{2a^2}{h^2+a^2+z^2} W^n - \frac{(4n+3)!!}{(n+1)(n!)^2\, 4^{2n}} \frac{W^n}{4} \right] \quad (22)$$

We can simplify the first term of the difference of summations using Stirling's approximation.

$$\lim_{n\to\infty}\frac{(4n+1)!!}{4^{2n}(n!)^2}=\lim_{n\to\infty}\sqrt{2(4n+1)}\left(\frac{4n+1}{e}\right)^{2n+1/2}\frac{2\pi n}{4^{2n}}\left(\frac{e}{n}\right)^{2n}\left(\frac{12n}{1+12n}\right)^{2}\to\frac{2\sqrt{2}}{\pi} \quad (23)$$

We note that the second term of the summation is identical to the series in the radial approximation.

$$B_z=\frac{\mu_0 I}{4(h^2+a^2+z^2)^{\frac{1}{2}}}\left[\frac{2a^2}{h^2+a^2+z^2}\sum_{n=0}^{\infty}\frac{2\sqrt{2}}{\pi}W^n-\sum_{n=0}^{\infty}\frac{8\sqrt{2}}{\pi}\frac{W}{4}^n\right] \quad (24)$$

The infinite series is a converging power series, and again we will solve for the k=0 term, and then assume that the coefficients in Eq. 24 are constant for the k>0 terms we arrive at the first order axially field solution.

$$B_z\approx\frac{\mu_0 I}{4(h^2+a^2+z^2)^{\frac{1}{2}}}\left[\frac{2a^2}{h^2+a^2+z^2}B_Z-\left(\frac{W}{4}\right)A_Z\right] \quad (25)$$

$$A_Z=3+A_{z1}\left(\frac{W}{1-W}\right)\qquad A_{Z1}=\frac{8\sqrt{2}}{\pi}\qquad B_Z=1+B_{Z1}\left(\frac{W}{1-W}\right)\qquad B_{Z1}=\frac{2\sqrt{2}}{\pi} \quad (26)$$

Since these two series have errors in opposite direction you must have them exactly fit at the current loop.

2.5 Axial Simulation

Similarly, to the radial component, Mr. Sahota and Dr. Chapman produced 2D plots for the axial field relative error in 2D. However, it is not possible to nicely plot the axial component in W space, so we can plot the relative error in the loop plane (z=0) without any curve fitting to the coefficients as shown in Fig. 11.

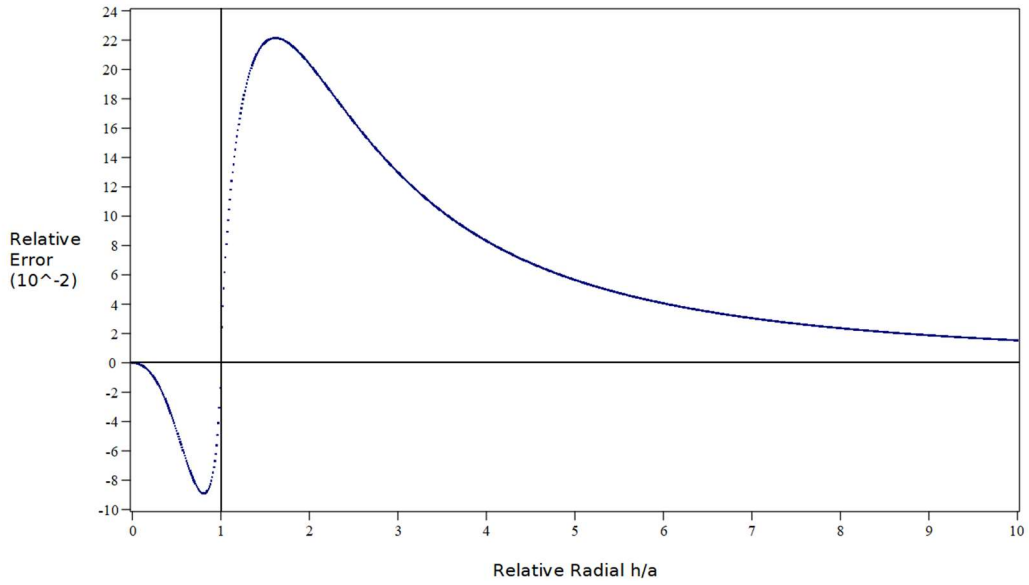

Fig. 5 First order relative error for the axial field in the loop plane (z=0).

We can curve fit the coefficients individually in this plane, by setting the approximation to be exactly correct at the loop, W=1 or (h,z) = (a,0). This uses 1 degree of freedom for our approximation, it is necessary to use the infinite terms of equation (23) so that the relative error for both A_Z and B_Z is zero at the current loop, which greatly reduces our accuracy. However, Fig. 5 shows that the accuracy of our first order approximation is already an order of magnitude larger than for the radial field – which is really caused by that loss of the degree of freedom. To significantly improve our accuracy, we need the additional degrees of freedom from higher ordered approximations. What this really says is the first order approximation for the axial field is not sufficiently accurate to be useful.

The axial plots in the loop plane are essential to fit coefficients for the approximation but does not let use visualize the behaviour of the axial approximation. Expanding our exploration to the relative error inside the loop (h<=a) in 3D space leads to the following plots

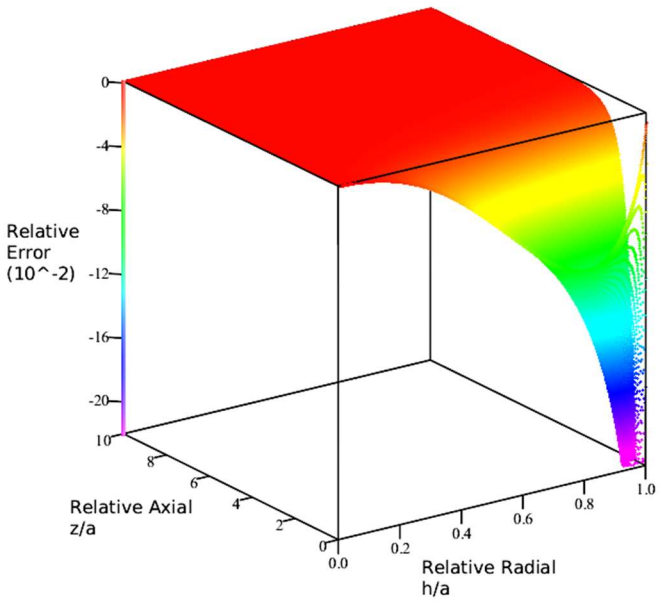

Fig. 6 First order relative error for the axial field approximation within the loop (h<=a).

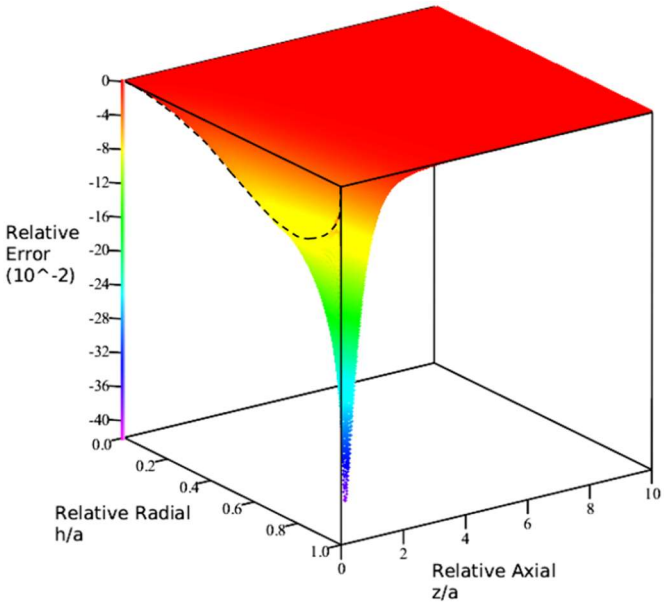

Fig. 7 First order axial approximation within the loop (h<=1) with the dashed black line showing the relative error in the loop plane (z=0)

Fig. 6 shows the relative error of the axial field approximation for distances less than the radius of the loop from the coil axis (h<=a). The approximation in this region is highly accurate with a downward spike in relative error as we approach the loop. This downward spike in relative error is also determined by the axial distance from the loop. The coefficients were fitted in the loop plane (z=0), and we've shown that in this plane, the maximum relative error is approximately 9%. However, as we move axially away from the loop there is a region where the relative error spikes downwards for small z. The relative error in the loop plane is shown as the dashed black line in Fig. 7, which shows that for small z near the loop (h -> a), the relative error spikes downwards to nearly -40%.

Expanding this exploration to include the region outside of the loop (h>a) results in the Fig. 8, which had some unexpected behaviour. Outside of the loop, we also see that the approximation is highly accurate at great distances from the loop. However, there appears to be a region where on one side the relative error spikes to negative infinity and on the other, spikes to positive infinity. This behaviour was causing the unexpected axial behaviour during early explorations. This result was unexpected, but using our 3D plotting it became better understood by the plot below, where we see a void of data points where the approximation's relative error appears to spike.

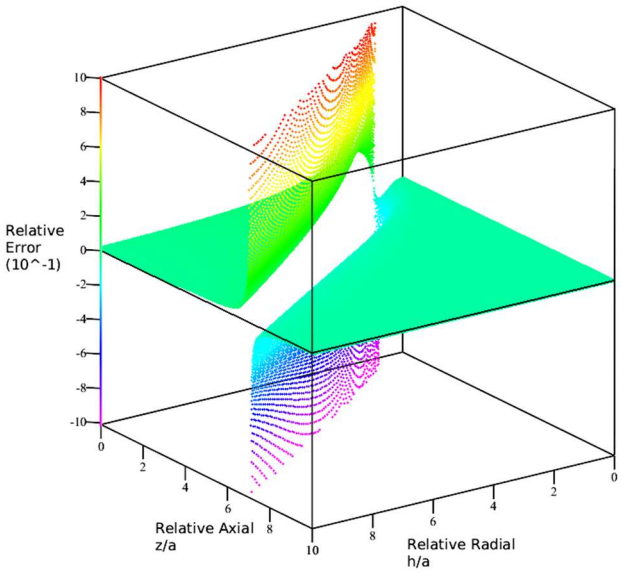

Fig. 8 First order axial field relative error.

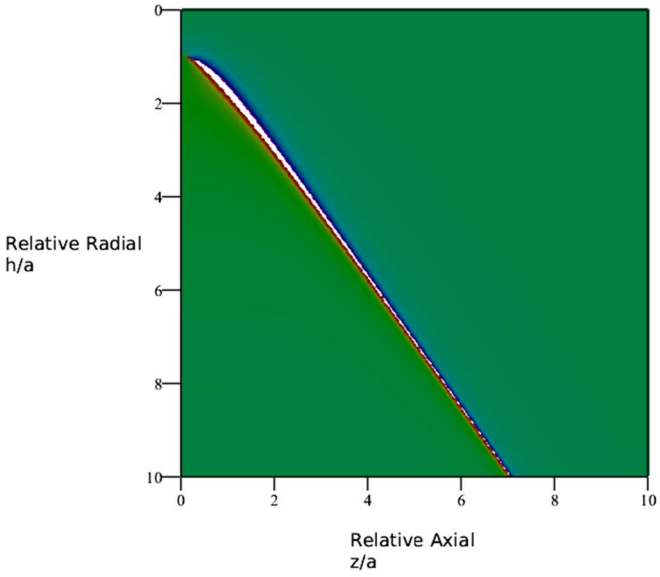

Fig. 9 First order axial field relative error top view.

The auxiliary views of the first order axial field in Fig. 8 and Fig. 9 show that there is a discontinuity in the relative error along a relatively linear region. This plot immediately showed that the bidirectional singularly likely occurs where the axial field reverses polarity. Exploration showed that this error exists at z elevations from the loop where the axial field declines to zero then reverses. This occurs as the h and z coordinates where the axial field reverses polarity differs slightly between the approximation and exact equations. This slight difference has a nearly negligible distance, actually far less Δz at any h>=1 than the relative error maximums within the loop. Due to this position error the absolute difference in the field is very small, but it leads to a relative difference of many orders of magnitude (i.e., if the true field is 0 but the approximation predicts a finite (but very small field) the error goes to infinity in both directions). To quantitatively explore this, we plotted the axial field zero locations of the approximation and analytic equations (h2, z2) as shown in Fig. 10.

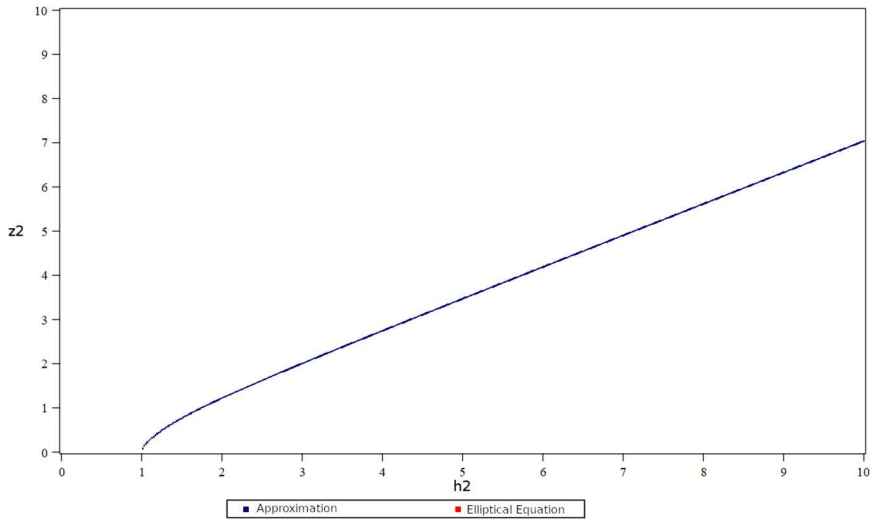

Fig. 10 Axial field zero locations for the 1st order approximation and elliptical equation

Which, as expected, showed that the points on the 2D plot in Fig. 10 match the shape of the void seen in Fig. 9. This confirmed that the large spikes in relative error occur at the location where the axial field changes sign. We also note that this plot has both the zero locations for the analytical elliptical and approximation equations, but they nearly perfectly overlap.

The previous explorations of the first order axial approximations left much to be desired. The limited degrees of freedom and spikes in relative error were not ideal, which lead to Mr. Sahota, in conjunction with Nick Pfieffer, developing a modified solution for the first order approximation by adding additional corrective terms and modifying the first order axial approximation (1st order radial remains unchanged). While this improvement does not carry over into the higher ordered approximations, Mr. Sahota's improvement curve fits additional degrees of freedom, by adding additional terms to minimize the maximum relative error in the loop plane. The improved first order approximation becomes the following with fitted coefficients [8].

$$B_z \approx \frac{\mu_0 I}{4(h^2+a^2+z^2)^{\frac{1}{2}}}\left[\frac{2a^2}{h^2+a^2+z^2} - \left(\frac{W}{4}\right) B_{zr}\right] B_{zl} \quad (27)$$

$$B_{zl} = 1 + A_{z1}\left(\frac{W}{1-W}\right) \; B_{zr} = \; 3 + A_{zr1}W + \; A_{z3}\left(\frac{W}{A_{zr2}-W}\right) \quad (28)$$

$$A_{z1} = 0.900316316157106 \qquad A_{zr1} = 0.577649074805133$$

$$A_{z3} = 0.0504096148351019 \qquad A_{zr2} = 1.11935481095926$$

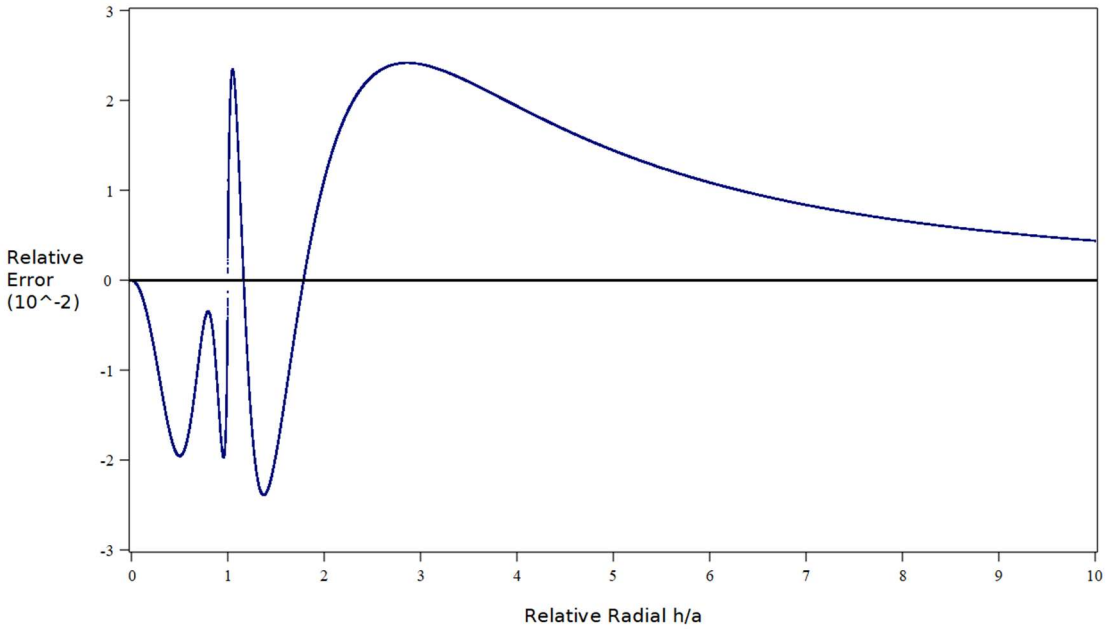

Fig. 11 Improved first order relative error for the axial field in the loop plane (z=0).

We can see that the Pfieffer – Sahota first order modification significantly improves the approximation and matches the 2 significant figure accuracy of the radial approximation for our first order approximations in the loop plane (z=0). However, this modification doesn't remove the spikes in relative error at the polarity changing locations. So, the resulting spatial 3D plot looks nearly identical, but with the relative error reduced by approximately a factor of 10. However, as we will see in Chapter 3, the increases in accuracy for higher order approximations significantly outperforms this modification.

2.6 Magnitude Simulation

Another way to visualize the behaviour of the approximation is by looking at the relative error of the magnitude of the magnetic field (Fig. *12*).

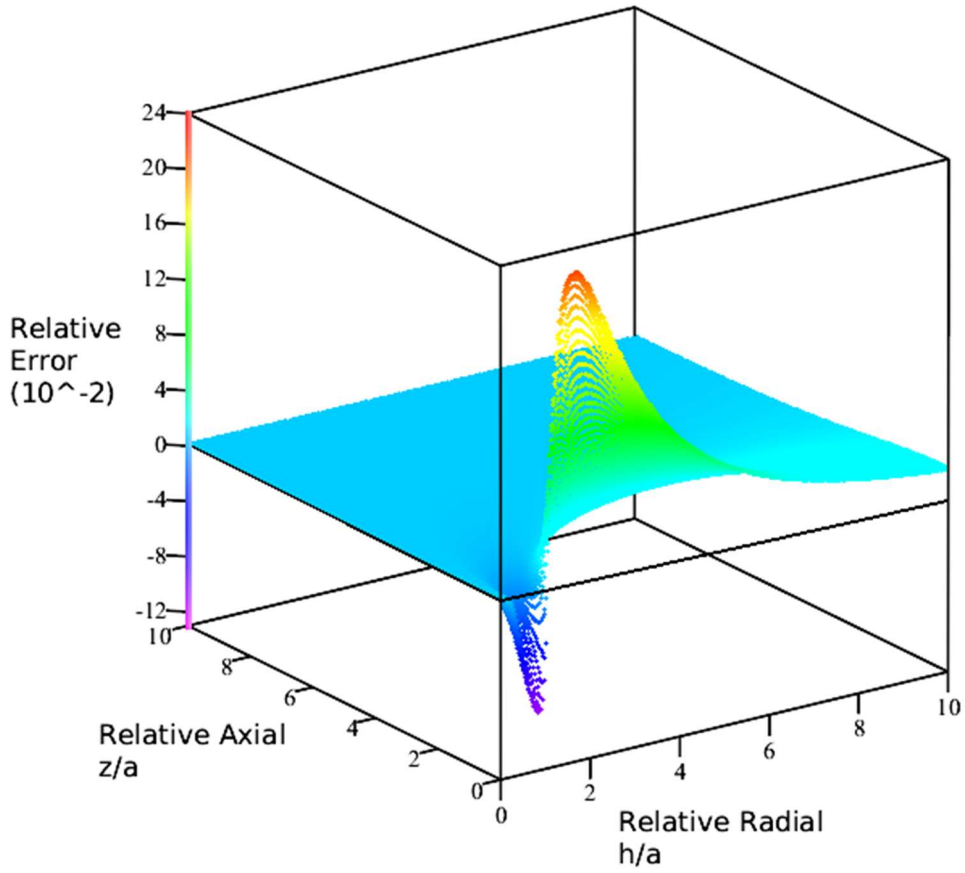

Fig. 12 First order relative error for the field magnitude.

The relative error in the magnitude is bounded across all space and notably follows the same relative error curve in the loop plane (z=0) as shown in Fig. 5. Notably, the only large fluctuations in the relative error are in or near this loop plane, whereas nearly everywhere else the approximation is highly accurate even at first order. The strength of the axial field is nearly negligible where its relative error diverges as the field is entirely dominated by its radial component. When visualizing the approximation behaviour from the magnitude, the issues with the axial approximation are negligible. Additionally, we can see in the magnitude plot the characteristic behaviours of the approximation when looking at regions where the

magnitude is dominated by the axial and radial fields respectively. This visualization also demonstrates the high accuracy of these approximations even for first order, although the magnitude does hide the direction of the field.

2.8 W, The Scaling Factor

During the derivation of the radial field, the scaling factor W, appears mathematically. The scaling factor is spatially dependent and depends on the size of the loop and has some physical significance. Rewriting W in the following form we can see it depends on the relative axial and radial coordinates of the system.

$$W = \frac{4h^2a^2}{(h^2+a^2+z^2)^2} = 4\left(\frac{h}{a}\right)^2 \frac{1}{\left[\left({}^{h}/_{a}\right)^2 + 1 + \left({}^{z}/_{a}\right)^2\right]^2} \quad (29)$$

We see that W is a dimensionless parameter involving the ratio of the relative radial distance (h/a) to the observation point and the scaled characteristic length [1 + (h/a)^2 + (z/a)^2]^(1/2). The scaled characteristic length has the form of a circle of radius a, which isn't surprising as the magnetic field is cylindrically symmetric for a current loop. Interestingly if we re-arrange the radial approximation by substituting another factor of W in front of the approximation term A_R, we get the following equation.

$$B_r \approx \frac{\mu_0 I}{4} \frac{z}{h\,(h^2+a^2+z^2)^{\frac{1}{2}}} \left(\frac{W}{4}\right) A_R \quad (30)$$

When the radial approximation is written in this form, we see that this is nearly identically the same term that appears in the axial approximation apart from a factor of z/h and the axially fitted coefficients in the A_R approximation term. This shows us the axial approximation can be effectively written as the difference of some function and a function of the same form as the radial approximation (with different fitted coefficients).

$$B_z \approx \frac{\mu_0 I}{4} \frac{\sqrt{h^2+a^2+z^2}}{2h^2} W B_z - \frac{z}{h} f(B_r) \quad (31)$$

We can now see the relationship between W and the axial and radial field components. While W may be a natural parameter to explore the behaviour of the current loop's magnetic field, it's behaviour across all space isn't obvious. We can plot the contour plots of W over all space, and show its special dependence as shown in Fig. 13.

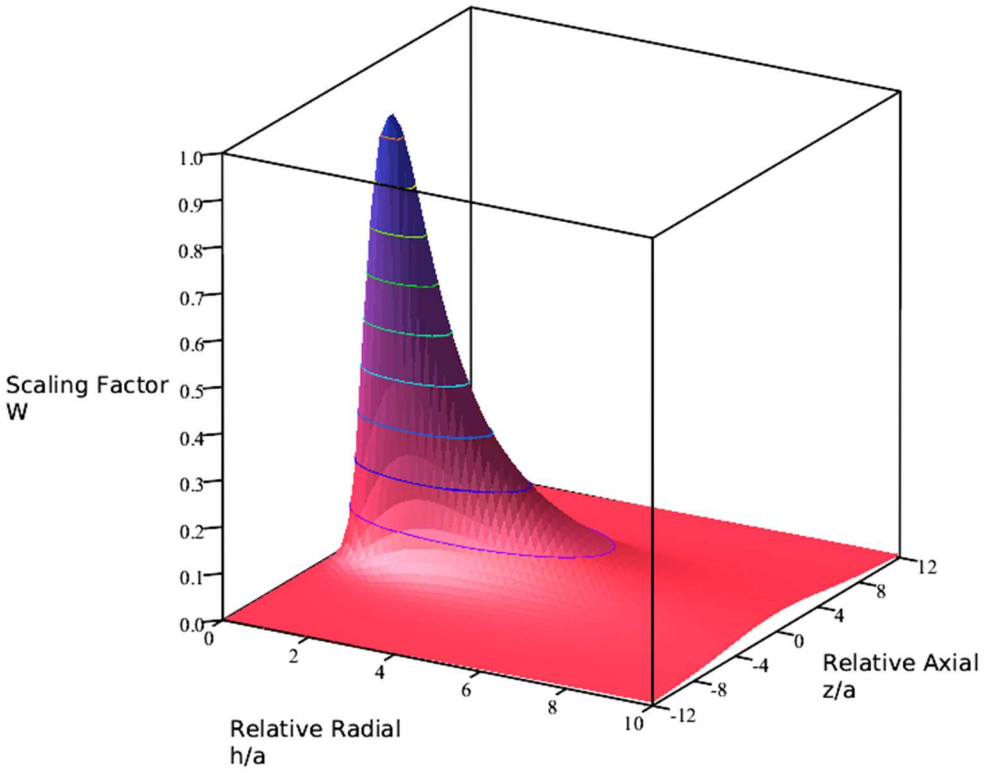

Fig. 13. Contours of W, the scaling factor.

The scaling factor, W, naturally appears during the mathematical derivation for both components of the cylindrically symmetric magnetic field and establishes a relationship between the axial and radial magnetic field approximations. While W appears mathematically, what it is physically is a difficult problem. We have explored what W is spatially as a dimensionless quantity as well as its relationship between the components of the magnetic field, but it could have more physical significance.

2.9 Comparison to Dipole Approximation

Another common approximation is the magnetic dipole approximation where we effectively treat the current loop as a point and calculate the magnetic field in the far field. This approximation is highly accurate if we are far enough from the loop to effectively treat it as a point. For the magnetic dipole approximation, we look at the limit where the current loop shrinks to a point, but has a constant magnetic moment, m. To evaluate the magnetic field at a point we consider a sphere of radius r centered on the magnetic point that extends to the evaluation point (Eq. 32)

$$B(R) = \frac{\mu_0}{4\pi}\left[\frac{3\hat{R}(\vec{m}\cdot\vec{R})}{R^5} - \frac{\vec{m}}{R^3}\right] \qquad (32)$$

However, while the dipole approximation is highly accurate in the plane of the loop (z=0) in the far field, its accuracy significantly diminishes in the mid to near field. Additionally, the dipole approximation along the especially important loop axis is also highly inaccurate (h=0) even in the far field, whereas all orders of our approximations are exactly correct along the coil axis. TABLES II, III, IV show the fractional relative error of the dipole and our approximations in the loop plane (z=0), along the loop axis (h=0), and along the vector [h=1, z=1], 45 degrees off the coil axis. For the loop plane (z=0) and along the coil axis (h=0) we note that the magnetic field should be entirely in the axial direction, however as discussed in section 2.2, the elliptical equations exhibit a strange behaviour for h=0, therefore we have fixed h at 0.01a.

P(h, z)	(0.01a, a)	(0.01a, 3a)	(0.01a, 5a)	(0.01a, 10a)
Dipole				
Axial (B_z) Relative Error	1.83	0.171	6.06×10^{-2}	1.50×10^{-2}
Direction Absolute Error	$0.430°$	$(2.86 \times 10^{-2})°$	$(6.46 \times 10^{-2})°$	$-(6.23 \times 10^{-4})°$
Binomial				
Axial (B_z) Relative Error	-3.72×10^{-6}	-1.48×10^{-7}	-1.65×10^{-8}	1.23×10^{-8}
Direction Absolute Error	$6.22° \times 10^{-6}$	$1.50° \times 10^{-6}$	$-1.51° \times 10^{-4}$	$-1.47° \times 10^{-3}$

TABLE II. Comparison between 1st order and dipole approximations along the loop axis (fixed h=0.01a).

Comparing the dipole and our first order approximations along the loop axis yield somewhat expected results. Our approximation is exactly correct along the coil axis, and the dipole approximation performs exceptionally poorly when we are close to the loop along the axis. Remembering that the dipole approximation assumes that the loop is a point and that the distance from this point is in the loop plane (z=0). The coil axis is 90° from the loop plane (z=0), so we expect the dipole approximation to perform relatively poorly everywhere in space with a relative error of approximately 1.5% at z=10a and 183% at z=a. Performing the same relative error comparison along the loop plane, where we expect the best performance from the dipole approximation is tabulated below in TABLE III. Notably, the directional accuracy of the dipole is quite poor, except in the loop plane (z=0).

P(h, z)	(1.5a, 0)	(3a, 0)	(5a, 0)	(10a, 0)
Dipole				
Axial (B_z) Relative Error	0.219	0.124	4.48×10^{-2}	1.12×10^{-2}
Direction Absolute Error	$0°$	$0°$	$0°$	$0°$
Binomial				
Axial (B_z) Relative Error	-0.480	-0.130	-5.65×10^{-2}	-1.15×10^{-2}
Direction Absolute Error	$0°$	$0°$	$0°$	$0°$

TABLE III. Comparison between 1st order and dipole approximations in the loop plane (fixed z=0).

In loop plane (z=0), the dipole approximation actually performs better than our 1st order approximation even when we are radially close to the loop. Expanding our comparison at a 45° angle from the centre of the coil, along the vector [h=1, z=1], yields the following results in TABLE IV.

P(h, z)	(a, a)	(3a, 3a)	(5a, 5a)	(10a, 10a)
Dipole				
Axial (B_z) Relative Error	-0.424	-0.116	-4.61×10^{-2}	-1.10×10^{-2}
Radial (B_r) Relative Error	0.457	2.07×10^{-2}	6.67×10^{-3}	1.59×10^{-3}
Direction Absolute Error	$21.7°$	$2.62°$	$0.945°$	$0.236°$
Binomial				
Axial (B_z) Relative Error	-7.25×10^{-2}	-3.93×10^{-2}	-1.69×10^{-2}	-4.56×10^{-3}
Radial (B_r) Relative Error	2.32×10^{-2}	7.03×10^{-3}	2.81×10^{-3}	7.36×10^{-4}
Direction Absolute Error	$2.74°$	$0.889°$	$0.353°$	$0.0921°$

TABLE IV. Comparison between 1st order and dipole approximations along the vector [1,1]

The radial field is nonzero at these locations resulting in an error in the field direction for both approximations. Overall, our approximation performs significantly better than the dipole approximation for both components of the field and a higher directional accuracy. Overall, our first order approximation is much more accurate than the dipole approximation everywhere in space, except along the coil axis where its accuracy is very comparable. However, our higher ordered approximations discussed in the next chapter increase the accuracy of our approximation by many orders of magnitude.

2.10 Summary

In summary, these first order approximations are both highly accurate and simple for the radial component with a maximum relative error of approximately 2.46%. The axial component is well behaved everywhere except near where the axial field reverses polarity, which has a negligible absolute error, but significant relative error. This occurs due to the slight difference in location where the field reverses polarity between the approximation and exact equations. However, for all other locations the first order approximation has both high relative and absolute accuracy. The greatest hindrance to the accuracy comes from the minimal degrees of freedom offered by the first ordered approximation. In the next chapter we will explore how the accuracy of the approximation increases as we gain additional degrees of freedom with higher order approximations.

Chapter 3. Higher Order Approximations

By repeating the process with higher binomial expansions combined with greater order Stirling's approximation applied to the factorial term series, we can improve the accuracy of the approximation. Adding the extra corrective terms to the approximation, provides additional degrees of freedom to fit the true field value. For first order, the radial approximation had 1 degree of freedom which we used to minimize maximum relative error. However, the axial approximation has zero degrees of freedom, which significantly limits its accuracy. However, as we expand into higher order approximations, we will gain additional degrees of freedom to force the approximation to be exactly correct at specific points of the system geometry.

For each higher order approximation, we performed the same curve fitting process, but with the additional degrees of freedom fitted to minimize the total relative error of the approximation. We will setup our curve fit to have n+1 peaks of equal height and n zero crossings for n degrees of freedom, which will achieve a high accuracy [10]. These additional corrective terms offer significant increases in accuracy while adding relatively low computational cost. The results of this process will be shown below for each order of the approximation.

3.1 Second Order Approximation

For the first order derivation, we evaluated the converging factorial series for an infinite number of terms in the factorials. For the factorial term in Eq. 17, we only use the first order Stirling's approximation, which is highly accurate for large n, but less so for small n. For example, while at n = 1 the first order Stirling has a 7.7% error from 1! , the second order Stirling (see Eq. 15) has only a 0.1% error which declines rapidly with higher n. Hence The second order term arise by re-examining this Eq. 16, using binomial expansion, which shows the need of adding corrective terms for small n of the form W/n and W/(n+1). In the limit as n goes to infinity, these coefficient terms converge to a constant, but we can add these terms to increase our accuracy for finite n by replacing them with their infinite series equivalent. This leads to two additional terms for the approximation terms that will improve the accuracy of the factorial term for smaller n [8].

$$\sum_{n=0}^{\infty} \frac{W^n}{n+1} = \frac{\ln(1-W)}{W} + 1 \qquad (33)$$

$$\sum_{n=0}^{\infty} \frac{W^n}{n} = \ln(1-W) \qquad (34)$$

Comparing the relative effect of these terms shows that the n+1 term dominates, hence our second order approximation will explore the dominant term which results in the following approximation terms.

$$A_R = \left[3 + A_{R1}\frac{W}{1-W} + A_{R2}\left(\frac{ln(1-W)}{W} + 1\right)\right] \qquad (35)$$

For the second order approximation, we will improve the accuracy over the first order approximation with two fixed endpoints with zero error, one at W=0 and the other at W=1. Then, performing the curve fitting

in the same manner as before where we use the additional degree of freedom to add another peak, and zero crossing, to the relative error and then equalize the maximum absolute relative error of approximation across all the peaks (Fig. 14). This additional term for the second order approximation provides an additional degree of freedom for our approximation. This equation is now minimized with the additional peak to yield the coefficients in Eq. 36.

Therefore, our second order approximation (Fig. 15) is exactly correct along the coil axis and at the loop with one additional oscillation in W of the relative error between these points as shown in Fig. 14. For the radial component, the coefficients were fitted in W space as it is simpler to visualize the peaks and maximum relative error [8]. This is a significant advantage of the second order approximation as our first order equation with two fixed endpoints had zero degrees of freedom. The following second order plots are the result of this process paired with their numerically fitted coefficients. Note in the 3D space plot of Fig. 11 the relative error oscillates close to the loop area but with this small error.

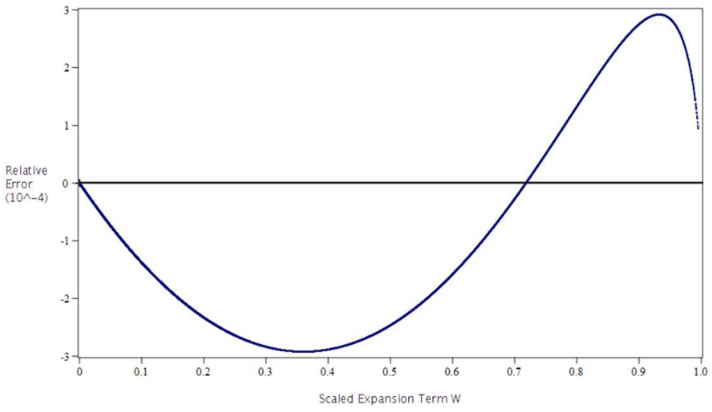

Fig. 14. Second order radial field relative error in W space with 1 degree of freedom

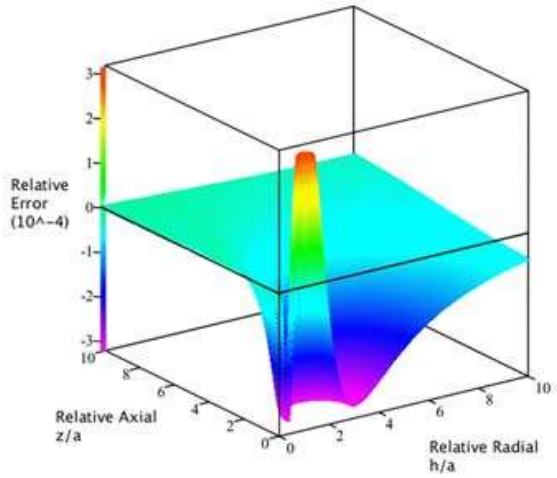

Fig. 15. Second order radial field relative error with maximum relative error of 2.9204×10^{-4}.

$$A_{R1} = \frac{8\sqrt{2}}{\pi} \qquad A_{R2} = 0.64955419888154950075 \qquad (36)$$

This improves our maximum radial field relative error to 2.9204×10^{-4} or approximately two orders of magnitude over the first order approximation. Applying the same method for the axial component, results in the following approximation terms with additional corrective terms of the same form.

$$A_Z = \left[3 + A_{z1}\frac{W}{1-W} + A_{z2}\left(\frac{ln(1-W)}{W} + 1\right)\right] \qquad (37)$$

$$B_Z = \left[1 + B_{z1}\frac{W}{1-W} + B_{z2}\left(\frac{ln(1-W)}{W} + 1\right)\right] \qquad (38)$$

When the curve fit is performed for the axial component, we are unable to fit in W space only because the A_z and B_z term subtraction/scaling in Eq. 25 means that off the loop plane there are many places with the same W but different relative error. However, we can apply the same methodology in the loop plane (z=0), where the field is strongest (and most important) we use the 3 extra degrees of freedom to make the approximation exactly correct at the centre of the loop, at the loop itself, and at an infinite distance from the loop [8]. Following this methodology results in the following plots. Note that because we are adding 2 coefficients for each higher order approximation (one in each of the A_z and B_z terms), we gain 2 degrees of freedom for each order of the axial approximation, as opposed to 1 additional degree of freedom for the radial approximation (the fits remove 1 degree of freedom). This higher degree of freedom in the 2nd order is why the axial relative error over 3 orders of magnitude, from the first order to an error close to that of the radial.

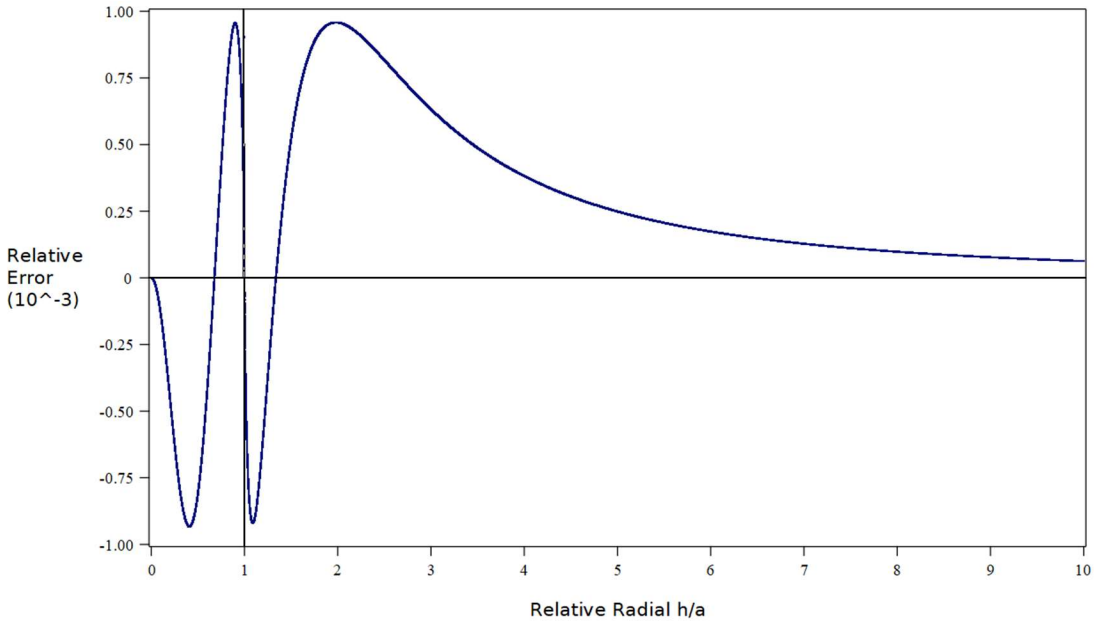

Fig. 16. Second order axial field relative error in the loop plane (z=0) with 2 degrees of freedom with a maximum relative error of 9.401×10^{-4}.

In the loop plane,
Fig. 16, we see that the 4 peaks and 5 troughs of the relative error are all of equal height and that the approximation is exactly correct at the center of the loop, at the loop itself, and that the approximation converges to exactly correct at far distances from the loop. These coefficients are given in Eq. 39 [8].

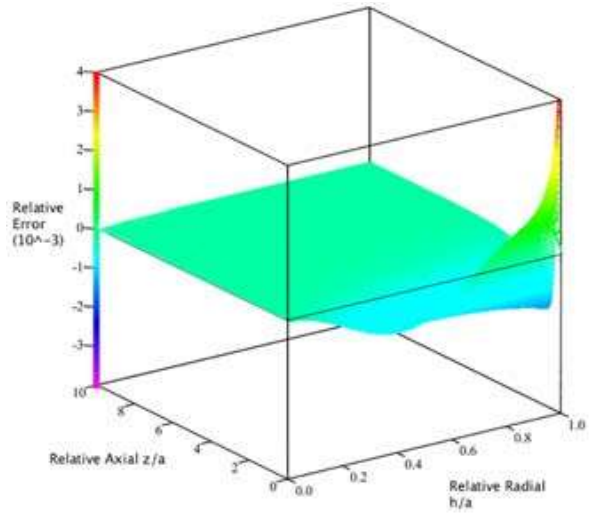

Fig. 17. Second order axial field relative error within the loop (h<=1).

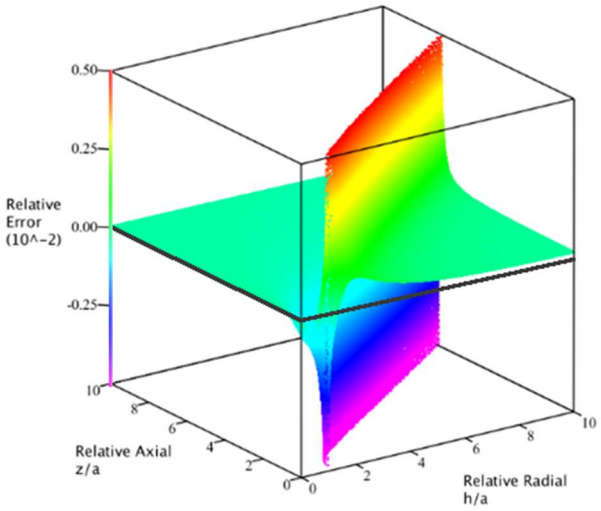

Fig. 18. Second order axial field relative error out to h=10 loop radii from its centre.

$$A_{Z1} = 3.6010098162048425 \qquad B_{Z1} = 0.9003002454051211$$
$$A_{Z2} = 0.6506161246955696 \qquad B_{Z2} = -0.0675136749142601 \qquad (39)$$

For the axial field, the primary region of interest is within the loop, and we can see in Fig. 17 that the approximation is well behaved every except as we approach the loop, $(h, z) \to (a, 0)$. Which is expected, as at the loop the magnetic field diverges at the loop for both the elliptical equations and the approximations. However, outside of the loop we encounter the same error as the axial field goes through a zero (reverses direction) as discussed for the first order approximation. The major improvement is that the relative error drops to zero much faster than first order – that is the positional error declines. Again, the relative error is effectively a small error in the actual location (h,z) of the axial field zero (where B_z reverses polarity) which follows the position shown in Fig. 10. The actual value of the field error is reduced by about 2 orders of magnitude, is has a relative error of about 10^{-3} compared to the axial field value at the loop plain, and for a given h the error is the z position of the zero crossing is reduced by about a factor of 100.

3.2 Third Order Approximation

For the third order, we can add the second term (W/n) from the second order Stirling's approximation/binomial expansion, which we neglected for the second order approximation [8].

$$\sum_{n=0}^{\infty} \frac{W^k}{k} = \ln(1 - W) \qquad (40)$$

$$A_R = \left[3 + A_{R1}\frac{W}{1-W} + A_{R2}\left(\frac{ln(1-W)}{W} + 1\right) + A_{R3}\ln(1 - \mathrm{W})\right] \qquad (41)$$

This grants for radial another degree of freedom, adding an additional peak and zero crossing in Fig. 19, in W space and enables us to add an additional constraint to force the approximation to be exactly correct at an infinite distance from the loop ($W \to 0$; $(h, z) \to \infty$) with corresponding fitted coefficients in Eq. 42 [8].

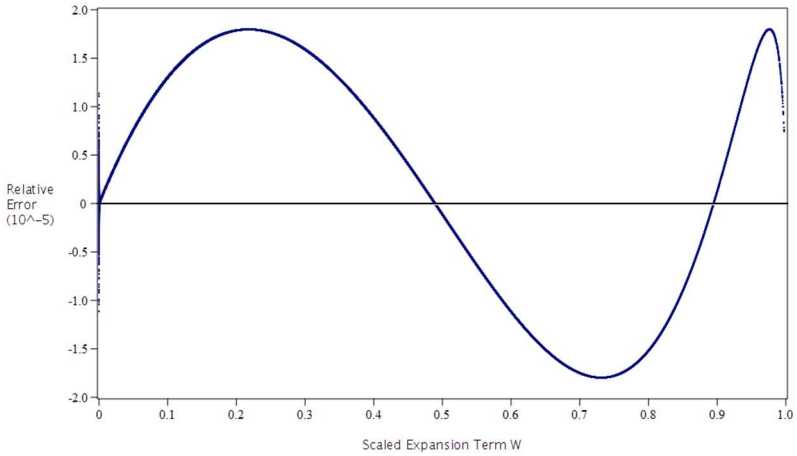

Fig. 19. Third order radial field relative error in W space with 2 degrees of freedom.

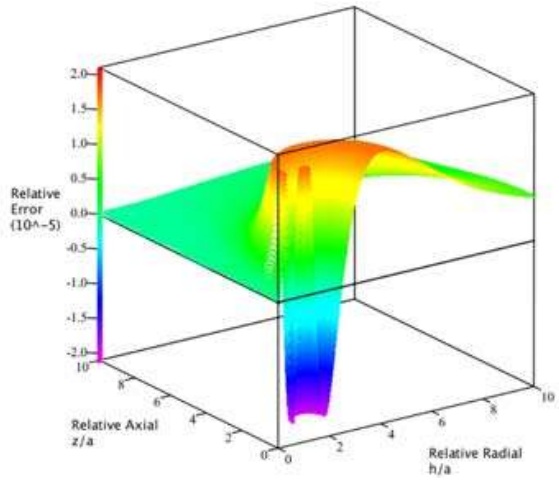

Fig. 20. Third order radial field relative error with maximum relative error of 1.797×10^{-5}.

$$A_{R1} = \frac{8\sqrt{2}}{\pi} \qquad A_{R2} = 0.70259705475849356 \qquad A_{R3} = -0.031808010186276496 \qquad (42)$$

Plotting in 3D space yields Fig. 20 where this additional degree of freedom reduces the maximum radial relative error by an additional factor of 50 to approximately 1.797×10^{-5}.

Following the same method for the axial field component, we get the following approximation terms (Eqs. 34 and 44) and fit the coefficients (Eq. 45) in the loop plane as shown in Fig. 21.

$$A_Z = \left[3 + A_{z1}\frac{W}{1-W} + A_{z2}\left(\frac{ln(1-W)}{W} + 1\right) + A_{z3}\ln\left(1-\mathrm{W}\right)\right] \qquad (43)$$

$$B_Z = \left[1 + B_{z1}\frac{W}{1-W} + B_{z2}\left(\frac{ln(1-W)}{W} + 1\right) + B_{z3}\ln\left(1-\mathrm{W}\right)\right] \qquad (44)$$

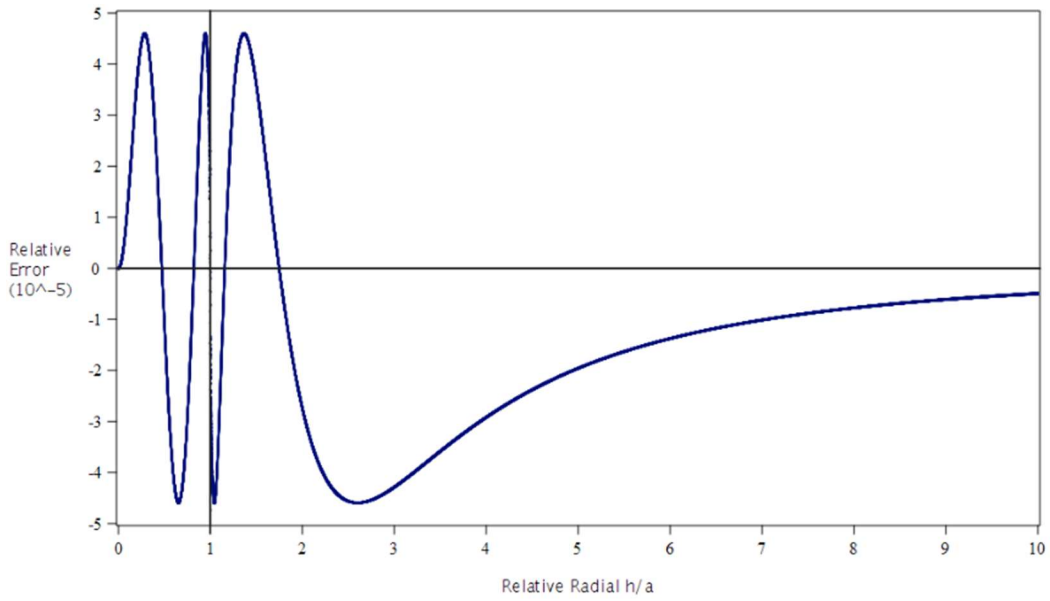

Fig. 21. Third order axial approximation in the loop plane (z=0) with 4 degrees of freedom with a maximum relative error of 4.594×10^{-5}.

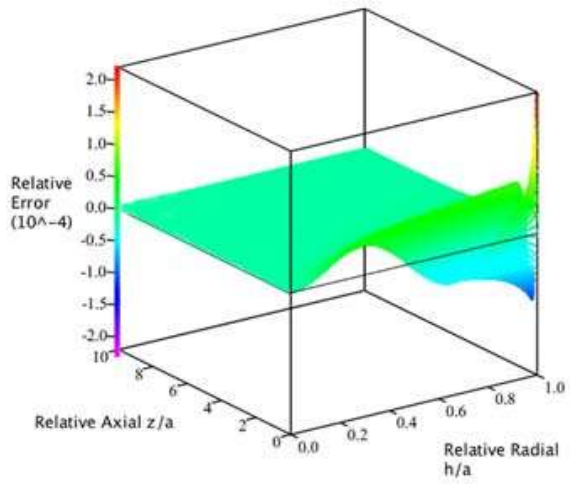

Fig. 22. Third order axial field relative error within the loop (h<=1).

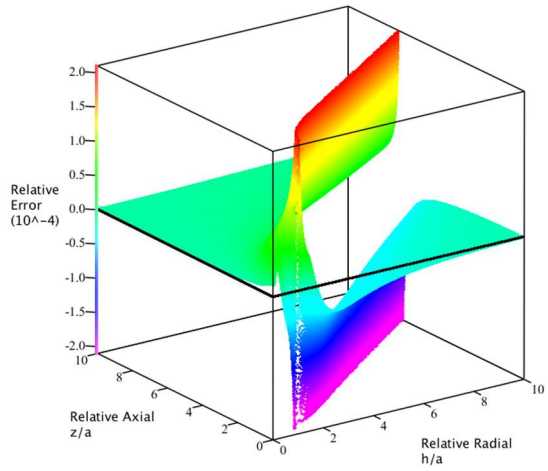

Fig. 23. Third order axial field relative error out to h=10 loop radii from its centre.

$$
\begin{aligned}
A_{Z1} &= 3.6012540756691833 & B_{Z1} &= 0.9003135189172958 \\
A_{Z2} &= 0.70316382703717930 & B_{Z2} &= -0.04053949010138328 \\
A_{Z3} &= -0.0321371127241916 & B_{Z3} &= -0.01725726367920613
\end{aligned}
\qquad (45)
$$

As Fig. 18 shows adding 2 more degrees of freedom gives us at the z=0 plane 6 relative error peaks and 7 zero crossings. For h<a, Fig. 19, the approximation continues to be well behaved except as we approach the loop. The third order approximation also continues to demonstrate the accuracy everywhere in space except near the axial field zero location (Fig.20), with the size of the absolute errors reducing by more than 10 and the accuracy of the field reversal location also improving.

3.3 Fourth Order Approximation

The second and third order approximations appeared after adding the second order Stirling's approximation expansions. However, adding an additional term with this method (third order Stirling and binomial expansion terms and cross products) would produce a term of the form.

$$\sum_{n=0}^{\infty} \frac{W^k}{k^2} \qquad (46)$$

These extra terms would likely improve the accuracy of the approximation, but to our knowledge functions of this form are not readily calculable. Rather, we know that the accuracy of Stirling's approximation is poorest for small n, but its accuracy rapidly increases with n. In Eq. 17, we are applying the second order Stirling's approximation to the factorial terms in the numerator and denominator. Referring to TABLE V below, we see that the relative error of Stirling's approximation is indeed highest for the n=1 terms of Eq. 17 with only a relative error of approximately 2% [8].

	n=1	n=2	n=3
Exact factorial value	3.28125	3.38379	3.43666
Stirling's approximation	3.21079	3.33642	3.40061
Percent Difference (%)	-2.14747	-1.39987	-1.04912

TABLE V. Stirling Approximation Errors for in Eq. 17.

Note that for the factorials in Eq 14, the first term of the double factorial in the numerator is 7!!, which means that Stirling's approximation of the numerator is highly accurate even for low values of n. Most of the error resides from the $1/(n!)^2$ term, as for small n squaring Stirling's approximation performs exceptionally poorly. Therefore, we will add an n=1 corrective term to compensate for the W^1 error to create the fourth order approximation (Eq. 47). Performing the curve fit in the same manner, yields the corresponding coefficients in Eq. 48.

$$A_R = \left[3 + A_{R1}\frac{W}{1-W} + A_{R2}\left(\frac{ln(1-W)}{W} + 1\right) + A_{R3}\ln(1-\mathrm{W}) + A_{R4}\mathrm{W}\right] \qquad (47)$$

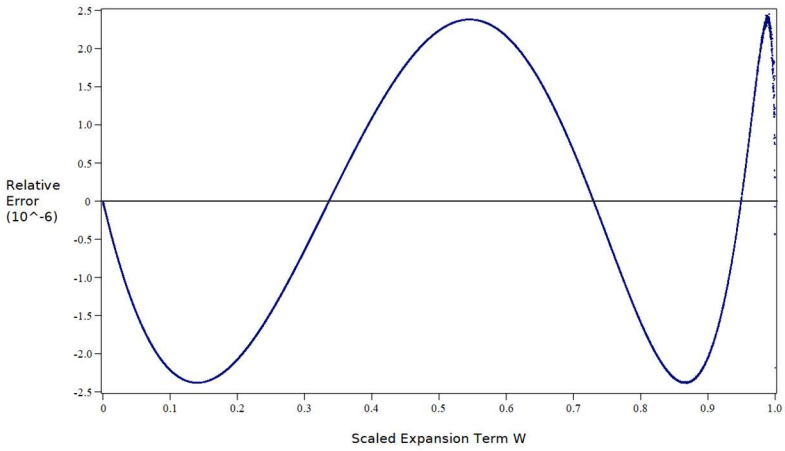

Fig. 24. Fourth order radial field relative error in W space with 3 degrees of freedom.

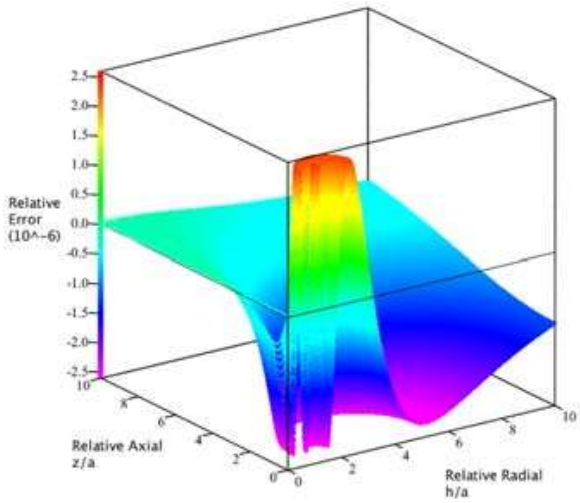

Fig. 25. Fourth order radial field relative error with maximum relative error of 2.381×10^{-6}.

$$A_{R1} = 3.60126526462842428 \qquad A_{R2} = 0.719522006152182159$$
$$A_{R3} = -0.04551153144606136 \qquad A_{R4} = -0.0058782306517071534 \qquad (48)$$

This additional degree of freedom creates (Fig. 24) 4 peaks and 5 zeros, thus reduces the maximum radial relative error by approximately an order of magnitude to approximately 2.381×10^{-6}. The fact that the improvement is so large shows just how rapidly the error on the Stirling/binomial approximation of the terms is decreasing, and hence the accuracy of the 1st to 3rd terms is improving. Fig. 25 shows the error is rapidly changing but very small near the loop.

When we first tried the fourth order approximation now introduces some noise in the 2D plot for W=0, corresponding the loop's axis and at an infinite distance from its centre for 3D plots. After much examination we set the approximation to be exactly correct at the loop axis, as it is clear this behaviour is unexpected, and we suspect this likely occurs as we approach the accuracy limit of Maple's built-in elliptical calculations. As this behaviour is likely occurring for similar reasons as the axial field zero, where there is a negligible absolute error, but a large relative error as our approximation and Maple's elliptical solver differs minutely. For the axial field component, we get the following approximation terms, Eqs. 49 and 50, when fitting in the loop plane with corresponding coefficients given in Eq. 51.

$$A_Z = \left[3 + A_{z1}\frac{W}{1-W} + A_{z2}\left(\frac{ln(1-W)}{W} + 1\right) + A_{z3}\ln(1-\mathrm{W}) + A_{z4}\mathrm{W}\right] \qquad (49)$$

$$B_Z = \left[1 + B_{z1}\frac{W}{1-W} + B_{z2}\left(\frac{ln(1-W)}{W} + 1\right) + A_{z3}\ln(1-\mathrm{W}) + B_{z4}\mathrm{W}\right] \qquad (50)$$

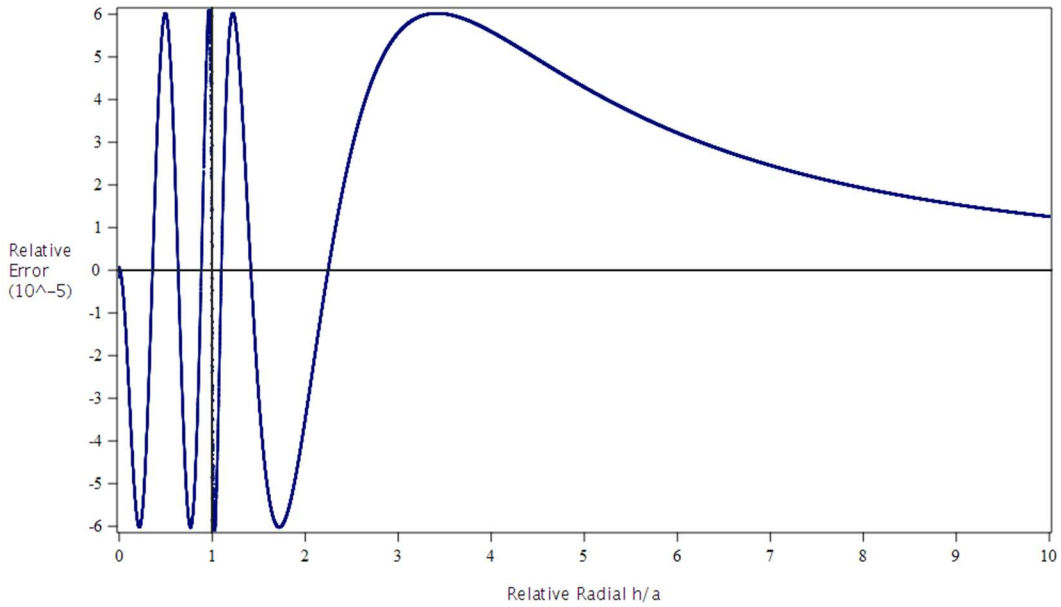

Fig. 26. Fourth order axial approximation in the loop plane (z=0) with 6 degrees of freedom with a maximum relative error of 6.022×10^{-5}.

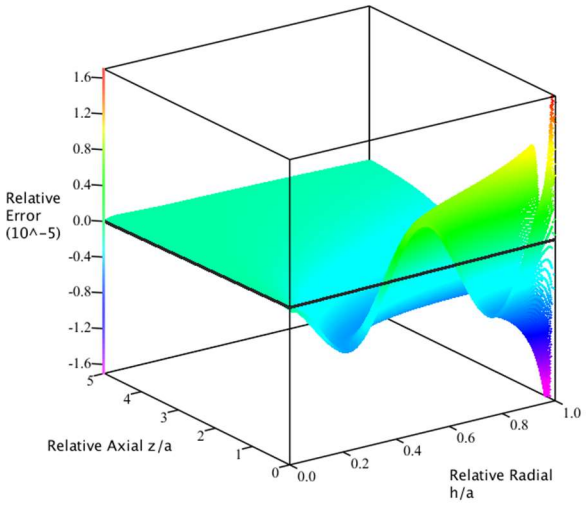

Fig. 27. Fourth order axial field relative error within the loop h<=1.

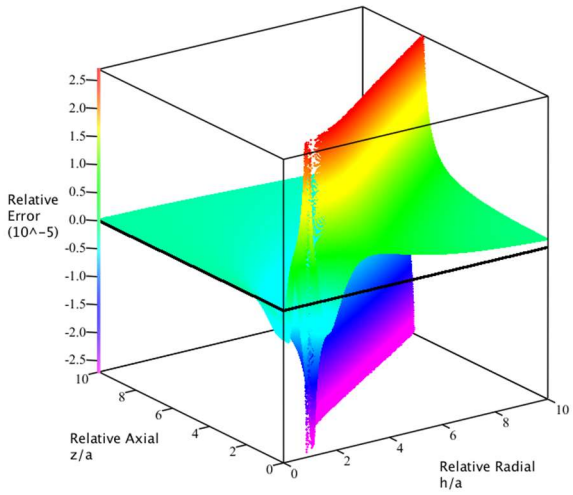

Fig. 28. Fourth order axial field relative error out to h=10 loop radii from its centre.

$$
\begin{aligned}
A_{Z1} &= 3.6012638273065052 \\
A_{Z2} &= 0.72013952447932811 \\
A_{Z3} &= -0.045997878241892 \\
A_{Z4} &= -0.00606243456599721
\end{aligned}
\qquad
\begin{aligned}
B_{Z1} &= 0.9003159568266263 \\
B_{Z2} &= -0.0333958397069874 \\
B_{Z3} &= -0.023244607318728 \\
B_{Z4} &= -0.002834921162840006
\end{aligned}
\qquad (51)
$$

The errors were well behaved at the loop plane (Fig. 26) where the increase in the degrees of freedom gives us 8 peaks and 9 zeros. For h<a, the accuracy of the fourth order axial approximation improves

another order of magnitude to approximately 6.022×10^{-6} and the difference in the axial zero location continues to improve. Hence the 3D plot in Fig. 28 looks much the same, but with sharper changes. As in lower order approximations the relative error is well behaved within the loop (Fig 24)

3.4 Fifth Order Approximation

The fifth order approximation follows the same method as fourth order, but we add a corrective term for n=2 term of the form W^2, which yields the following approximation function of Eq. 52 and coefficients in Eq. 53 to have zeros again at W=0 and 1 as shown in the W space plot of Fig. 29 with its corresponding 3D special behaviour shown in Fig. 30 [8].

$$A_R = \left[3 + A_{R1}\frac{W}{1-W} + A_{R2}\left(\frac{ln(1-W)}{W} + 1\right) + A_{R3}\ln(1-\mathrm{W}) + A_{R4}\mathrm{W} + A_{R5}\mathrm{W}^2\right] \qquad (52)$$

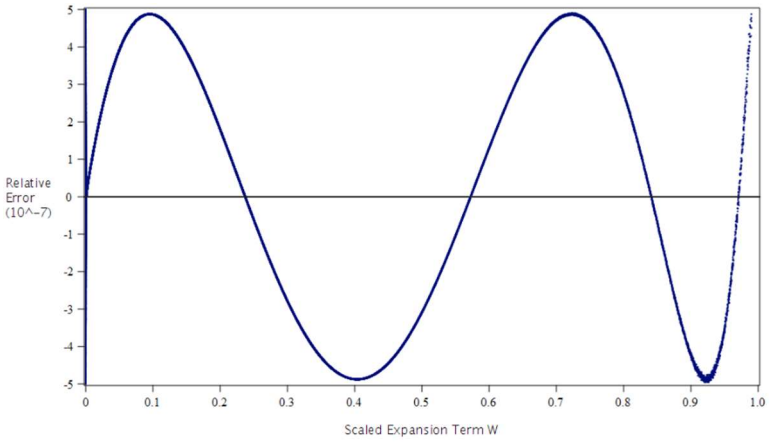

Fig. 29. Fifth order radial field relative error in W space with 4 degrees of freedom.

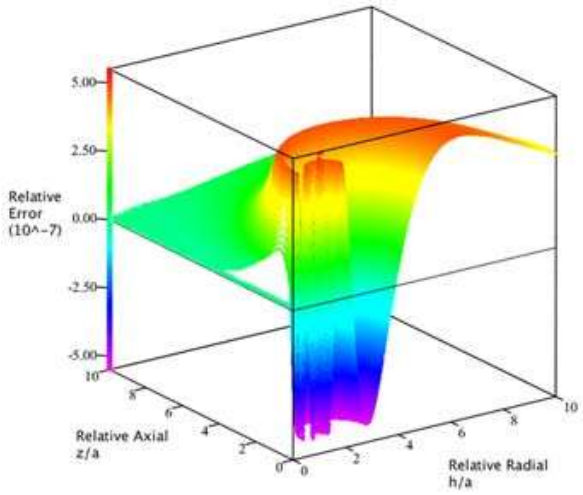

Fig. 30. Fifth order radial field relative error with maximum relative error of 4.876×10^{-7}.

$$A_{R1} = 3.60126526462842428 \qquad A_{R2} = 0.727021564606502388$$
$$A_{R3} = -0.008695310845331860 \qquad A_{R3} = -0.0522255035327797 \qquad (53)$$
$$A_{R5} = -0.0014574683941872$$

For fifth order, the maximum radial relative error is reduced by only half an order of magnitude to approximately 4.876×10^{-7} or 6 significant figures. Note in Fig. 26 that the error oscillates in the space around the loop, and at a distance from the loop at with that low maximum value. We continue to see the same relative approximation error at W=0 but is now more prevalent as the number of points has increased with the accuracy of the approximation.

For the axial field component, we again add a W^2 term to both A_Z and B_Z in Eqs. 49 and 50 to get the fifth order approximation terms (Eqs. 54 and 55) with corresponding approximation coefficients in Eq. 55 when curve fitting in the loop plane.

$$A_Z = \left[3 + A_{z1}\frac{W}{1-W} + A_{z2}\left(\frac{ln(1-W)}{W} + 1\right) + A_{z3}\ln(1-\mathrm{W}) + A_{z4}\mathrm{W} + A_{z5}\mathrm{W}^2\right] \quad (54)$$

$$B_Z = \left[1 + B_{z1}\frac{W}{1-W} + B_{z2}\left(\frac{ln(1-W)}{W} + 1\right) + A_{z3}\ln(1-\mathrm{W}) + B_{z4}\mathrm{W} + B_{z5}\mathrm{W}^2\right] \quad (55)$$

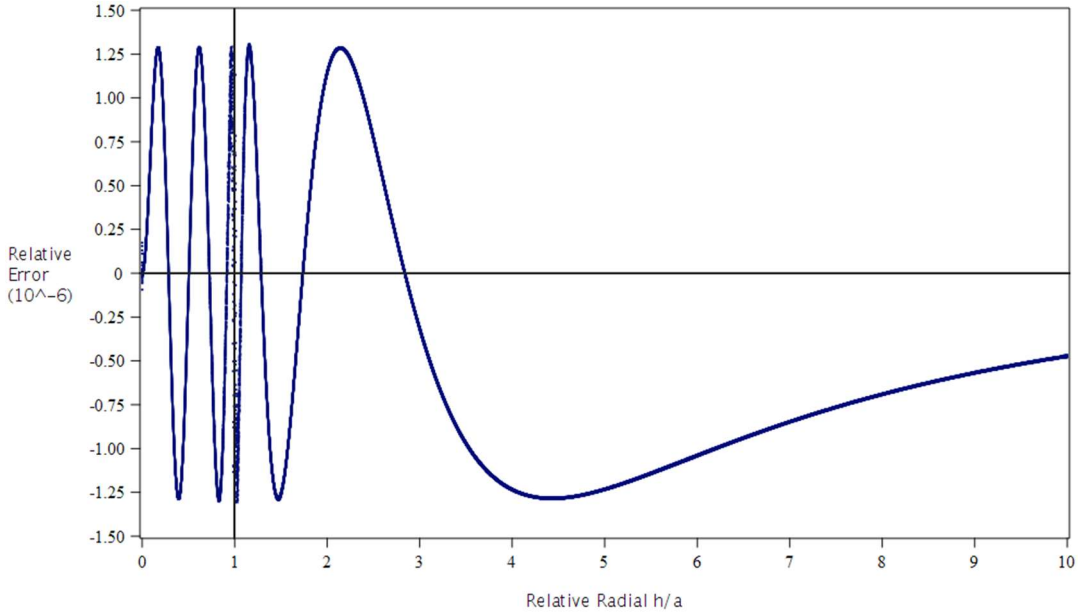

Fig. 31. Fifth order axial approximation in the loop plane (z=0) with 8 degrees of freedom with a maximum relative error of 1.293×10^{-6}.

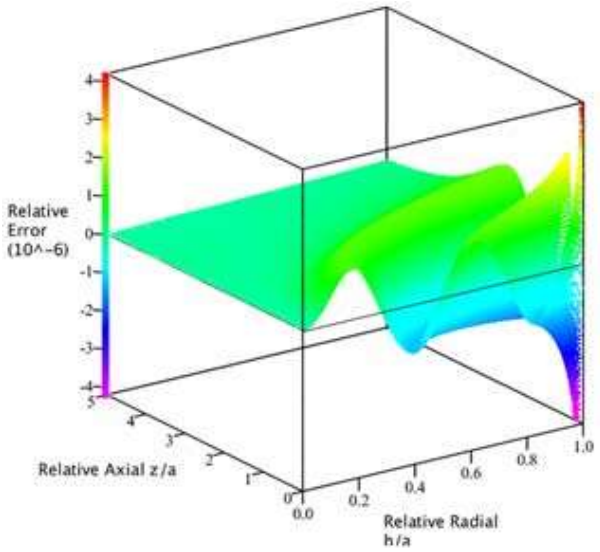

Fig. 32. Fifth order axial field relative error within the loop.

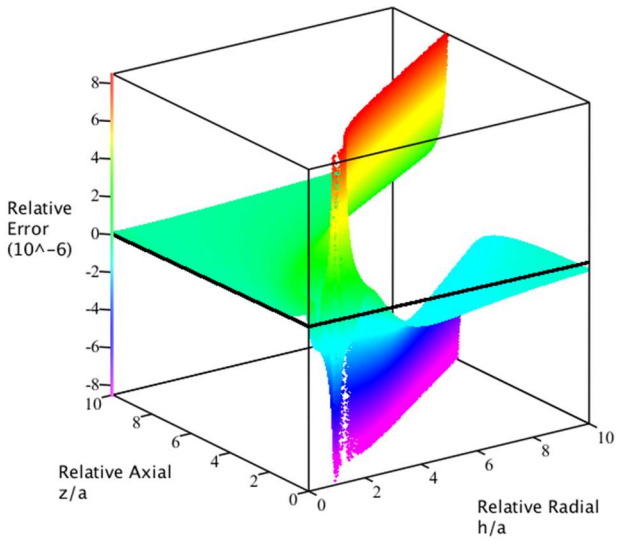

Fig. 33. Fifth order axial field relative error out to 10 loop radii from its centre.

$$
\begin{aligned}
A_{Z1} &= \ 3.6012649981533775 & B_{Z1} &= \ 0.9003162495383443 \\
A_{Z2} &= \ 0.7276276696916009 & B_{Z2} &= -0.03044435633189330 \\
A_{Z3} &= \ 0.0527599282256922 & B_{Z3} &= -0.025946696478408 \\
A_{Z4} &= -0.00892318142802500 & B_{Z4} &= -0.0039595895609185077 \\
A_{Z5} &= -0.0015500658123898 & B_{Z5} &= -0.0007177536438
\end{aligned}
\qquad (56)
$$

The axial fifth order improves upon fourth order by half an order of magnitude with a maximum relative error of 1.293×10^{-6}. At this point we now have 10 peaks and 11 zeros (see Fig. 28). Fig. 29 shows the relative error when we are less than the coil's radius away from the axis (h<a) and we see that the error oscillates near the loop plain but falls off rapidly as z increases. Again Fig. 30 shows the same issue as the other orders as the axial field reverses due to the error in the coordinates of the zero crossing, which at by now has at worse a 10^{-6} displacement in z for a given h. At this point the accuracy of the corrections is decreasing, and the magnitude of the worst-case care so small there seems little gain in continuing. Moreover, from a practical point of view we are reaching the complete limits of our ability to calculate the true value with the elliptical equations and do additional fitting of parameters.

3.5 Summary

Higher ordered approximations would likely continue to improve the accuracy of the approximation, however there is room to explore the alternative corrective terms for these terms. There is also room to re-examine the fourth and fifth order approximations to find a more mathematically rigorous way to improve the accuracy beyond adding corrective terms for the weaker terms of Stirling's approximation (i.e., Eq. 46 can be approximated). However, these approximations as they stand are highly accurate for most applications and our plots demonstrate their effectiveness. One alternative solution quotes a best-case accuracy of approximately 1% at h=0.8a, which is significantly larger error than even our second order approximation. This solution is also highly complex and requires the calculation many higher order derivatives to achieve this accuracy [6]. Additionally, increasing the accuracy also increases the computational cost and for many applications the simplicity of these equations are their biggest strength. The improvement in accuracy begins to decline at the fourth order approximation, possibly due to the method used to add the additional corrective terms, which suggests that the increase in accuracy may not be worth the added computational cost for most purposes. The radial component of the third order approximation is accurate to 4 significant figures across all space. Additionally, at the location where the axial field reverses polarity, the relative error may be substantial, the absolute error is negligible, and the axial approximation is highly accurate across all space.

In the next chapter we will apply the approximations of chapters 2 and 3 a simple but common design problems – the Helmholtz coil.

Chapter 4. Helmholtz Coil Applications

A classic engineering problem is designing a magnetic coil system to measure the properties of a material within a magnetic field. These characteristics include magnetic intensity, susceptibility, retentivity, and coercivity. In particular, a Helmholtz coil is commonly used to permanently magnetize material, measure their magnetic properties, or calibrate magnetic sensors. The Helmholtz Coil is one of the simplest methods to create a highly uniform volume of magnetic field. The Helmholtz coil is a system of two identical coils separated by a distance equal to their radii creating the near uniform magnetic field lines at the mid plane shown in Fig. 34. This system is a common engineering system to create a large volume with a highly uniform axial field and is used by the National Institute of Standards and Technology (NIST) to calibrate magnetometers [11].

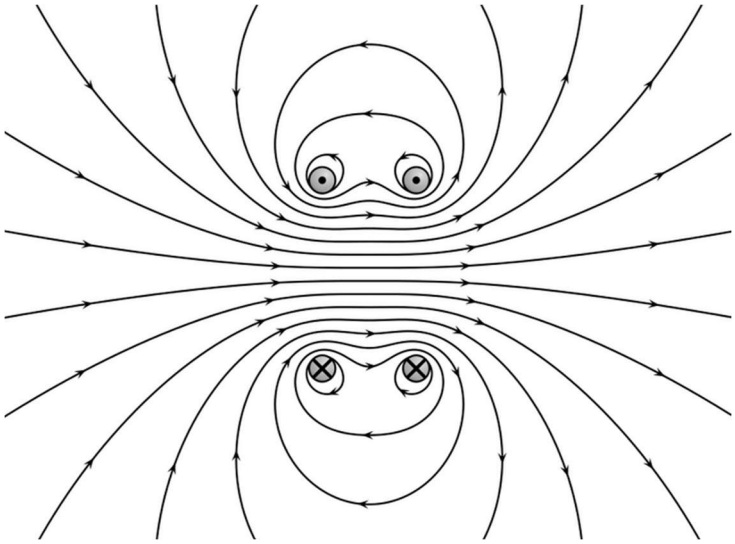

Fig. 34. Helmholtz coil cross section magnetic field lines [12].

Measuring the magnetic properties of a material require a highly uniform and magnetic field across the material as the accuracy of the measurements rely on the uniformity of the field. The easiest method is to simply make the coil's significantly larger than the target material, but deriving the required coil size for a specific field uniformity is a computationally difficult problem. In this chapter, we explore how well the new approximations work for this classic coil design problem.

Simulating the field from the elliptical equations, shown below in Eqs. 57, 58, results in in Figs. 32, 33, with each coil a distance equal to half their radii from the origin (system midplane at z=0).

$$B_r^H = \frac{\mu_0 I}{2\pi}\int_0^{\pi}\left[\frac{\left(z-\frac{a}{2}\right)a\,cos(\phi)}{\left(h^2+a^2+z^2-2ha\,cos(\phi)\right)^{3/2}} - \frac{\left(z+\frac{a}{2}\right)a\,cos(\phi)}{\left(h^2+a^2+z^2-2ha\,cos(\phi)\right)^{3/2}}\right]d\phi \qquad (57)$$

$$B_z^H = \frac{\mu_0 I}{2\pi}\int_0^{\pi}\left[\frac{\left(a^2 - ha\,cos(\phi)\right)}{\left(h^2 + a^2 + \left(z - \frac{a}{2}\right)^2 - 2ha\,cos(\phi)\right)^{(3/2)}} + \frac{\left(a^2 - ha\,cos(\phi)\right)}{\left(h^2 + a^2 + \left(z + \frac{a}{2}\right)^2 - 2ha\,cos(\phi)\right)^{(3/2)}}\right]d\phi \quad (58)$$

We can visualize the behaviour of the Helmholtz coil field from these equations with a Maple simulation using the elliptical integrals as shown in Fig. 35 and Fig. 36. We see that the radial field is exactly zero along the coil axis and then increases as we move away from the axis. We see that the radial field is relatively negligible when compared to the axial field unless we are near the coils (h > 0.8a). For both the axial and radial fields the field strength diverges as we approach the coil, which is clear from inspecting the denominator of the first order approximation and with greater difficulty, the elliptical equations. The axial field is very uniform along the coil axis and at the midplane of the coils (z=0).

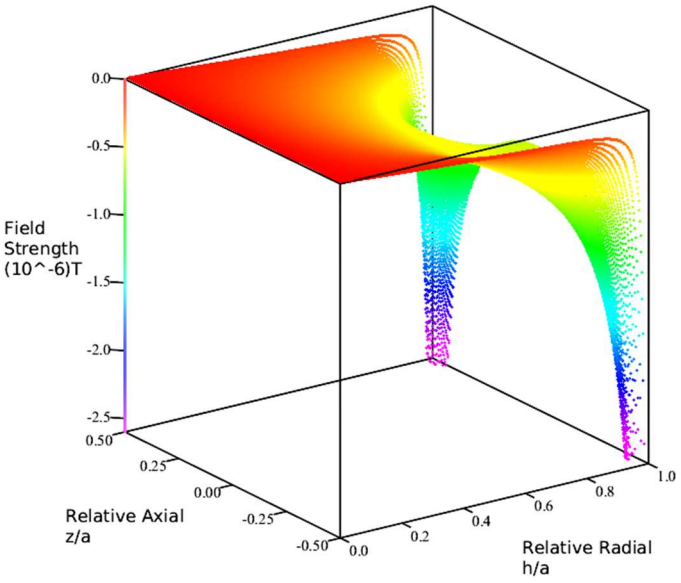

Fig. 35. Helmholtz Coil radial field strength from elliptical equations.

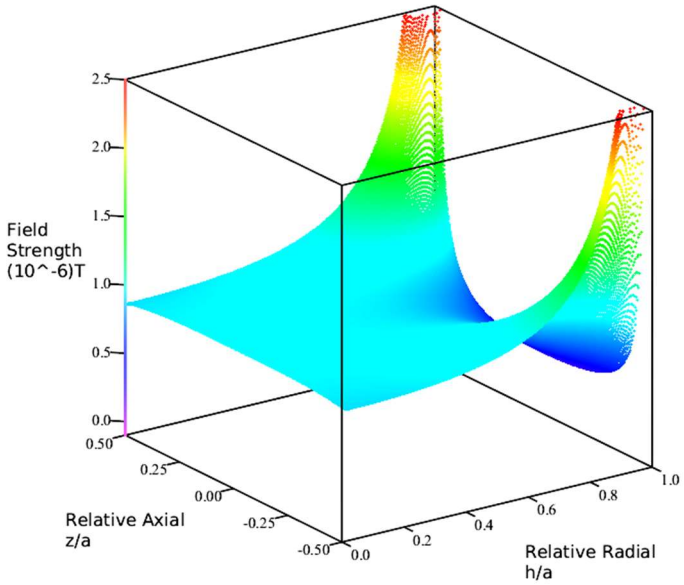

Fig. 36. Helmholtz Coil axial field strength from elliptical equations.

The Helmholtz coil spacing is analytically derived to produce a field that is uniform along the coil axis (z axis). The traditional method to solve for the coil separation is to place on coil at the origin and one coil at a distance, d, along the z-axis. Then, if we solve for, d, such that the first and second derivative of the axial field along the axis are zero, then one finds that the coil spacing is equal to the coil radius.

$$\left[\frac{\partial B_z^H}{\partial z}\right]_{h=0} = 0 \quad (59) \qquad \left[\frac{\partial^2 B_z^H}{\partial z^2}\right]_{h=0} = 0 \quad (60)$$

Satisfying these conditions with the elliptical integral equations is possible along the coil axis, but requires some minor integration, and is somewhat tedious. Alternatively, we could use our approximations to establish the same coil spacing in the same manner. Our approximations are exactly correct along the axis

regardless of the order of approximation. Using the first order axial field approximation in Eq 22, we set up our axial field equation as follows.

$$\begin{aligned} B_z^H &= B_Z(z,h) - B_Z(z-d,h) \\ &= \frac{\mu_0 I}{4\left(h^2+a^2+z^2\right)^{\frac{1}{2}}}\left[\frac{2a^2}{h^2+a^2+z^2}B_Z - \left(\frac{W}{4}\right)A_Z\right] \\ &\quad - \frac{\mu_0 I}{4\left(h^2+a^2+(z-d)^2\right)^{\frac{1}{2}}}\left[\frac{2a^2}{h^2+a^2+(z-d)^2}B_Z - \left(\frac{W}{4}\right)A_Z\right] \end{aligned} \quad (61)$$

The approximation terms A_z and B_z and the scaling factor, W, need to be calculated for each coil. However, along the coil axis (h=0), the W terms are zero and the approximation terms for each coil are identical, which means that our field equations simply nicely and we are left with the following equation for the first derivative.

$$\left[\frac{\partial B_z^H}{\partial z}\right]_{h=0} = \frac{-5I\mu_0 a^2}{4}\left[\frac{z}{(a^2+z^2)^{\frac{5}{2}}} + \frac{(z-d)}{(a^2+(z-d)^2)^{\frac{5}{2}}}\right] = 0 \;\rightarrow\; d = 2z \quad (62)$$

Which gives us a relationship between the coil spacing and the axial distance, solving the second derivative equation relates this to the coil radii, where we sub in the relationship above in Eq 55.

$$\left[\frac{\partial^2 B_z^H}{\partial z^2}\right]_{h=0} = \frac{-5I\mu_0 a^2}{4}\left[\frac{a^2-4z^2}{(a^2+z^2)^{\frac{7}{2}}} + \frac{a^2-4(z-d)^2}{(a^2+(z-d)^2)^{\frac{7}{2}}}\right] = 0 \;\rightarrow\; d = \pm a \quad (63)$$

We now explicitly see that this spacing was chosen to minimize any deviation of the axial field from the axis through the center of the coils. We also note that along this axis the radial field component from each coil is equal and opposite. Therefore, general equation for the Helmholtz coil approximations becomes the following.

$$B_r^H \approx \frac{\mu_0 I a^2 h}{4}\left[\frac{\left(z-\frac{a}{2}\right)^2}{\left(h^2+a^2+\left(z-\frac{a}{2}\right)^2\right)^{\frac{5}{2}}}A_R^+ - \frac{\left(z+\frac{a}{2}\right)^2}{\left(h^2+a^2+\left(z+\frac{a}{2}\right)^2\right)^{\frac{5}{2}}}A_R^-\right]$$

$$\begin{aligned} B_z^H &\approx \frac{\mu_0 I}{4\left(h^2+a^2+\left(z-\frac{a}{2}\right)^2\right)^{\frac{1}{2}}}\left[\frac{2a^2}{h^2+a^2+\left(z-\frac{a}{2}\right)^2}B_Z^+ - \left(\frac{W^+}{4}\right)A_Z^+\right] \\ &\quad - \frac{\mu_0 I}{4\left(h^2+a^2+\left(z+\frac{a}{2}\right)^2\right)^{\frac{1}{2}}}\left[\frac{2a^2}{h^2+a^2+\left(z+\frac{a}{2}\right)^2}B_Z^- - \left(\frac{W^-}{4}\right)A_Z^-\right] \end{aligned} \quad (64)$$

Where the + and – superscripts represent the coil to the right and left of the midplane respectively for the W and approximation terms.

$$W^{\pm} = \frac{4h^2a^2}{\left(h^2 + a^2 + \left(z \mp \frac{a}{2}\right)^2\right)^2} \qquad (65)$$

Therefore, the field between the pair of coils is uniform and is well suited for applications required a nearly constant magnetic field. If the application requires a highly uniform field across a specific volume, an engineer may want to model the system first. As we discussed in early chapters, calculating the off-axis magnetic fields are numerically expensive to calculate. However, when modelling these systems there is a trade-off between computational accuracy and its cost. The optimal solution is to find the minimal viable accuracy with the quickest computational time. Ultimately, the designer should choose the approximation which provides the required accuracy. However, as we have seen, the increase in accuracy drops diminishes with higher ordered approximations. The second order approximation improves the accuracy of the approximation by 2 orders of magnitude and may be the sweet spot for high accuracy and low computational cost. We also note that the second and third ordered approximations are derived from binomial expanding higher ordered Stirling's approximations, whereas the fourth and fifth order arise from adding additional corrective terms. This change of methods may reduce the improvement in accuracy from third to fourth order, and it is suspected that further exploration of higher ordered Stirling's approximations may produce a better approximation.

To find the sweet spot for accuracy and computational cost, we can explore the relative contributions of the approximation terms of chapter 3 approximations for each order of the approximations. If we compare the relative error of the lower ordered approximations to the highest order approximation (5^{th} order) which has a relative error of $1.2\text{x}10^{-6}$, we can visualize the effect of the higher ordered terms with the following equations.

$$RE_{Ar_i} = \frac{Ar_i - Ar_5}{Ar_5} \quad ; \quad RE_{Az_i} = \frac{Az_i - Az_5}{Az_5} \quad ; \quad RE_{Bz_i} = \frac{Bz_i - Bz_5}{Bz_5} \quad ; \quad i = 1..4 \qquad (66)$$

We can plot these equations by visualize the relative contributions of each order of our approximations with the following plots in Fig. 37 and Fig. 38.

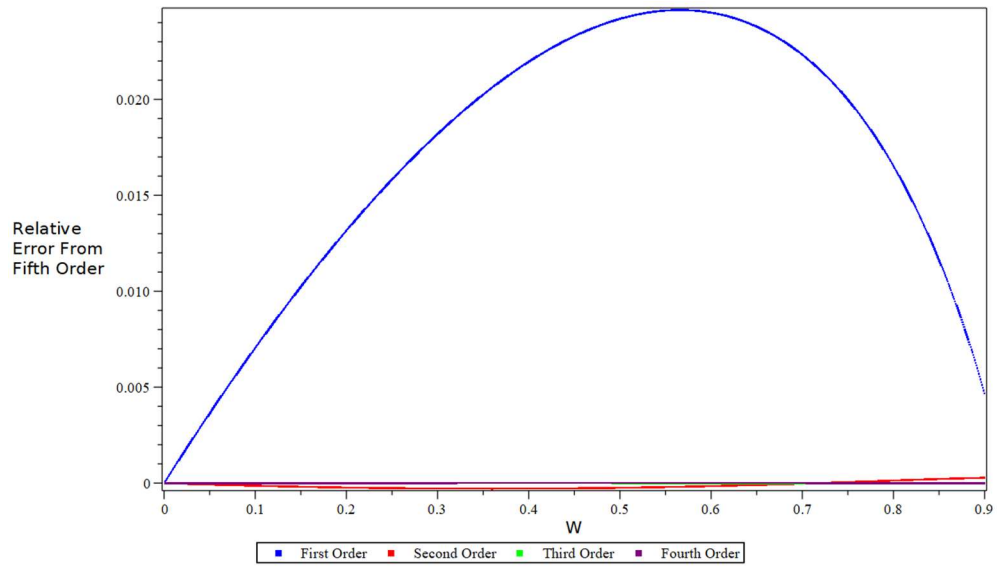

Fig. 37. Relative error of each ordered radial approximation term, A_r, to the 5th order approximation term.

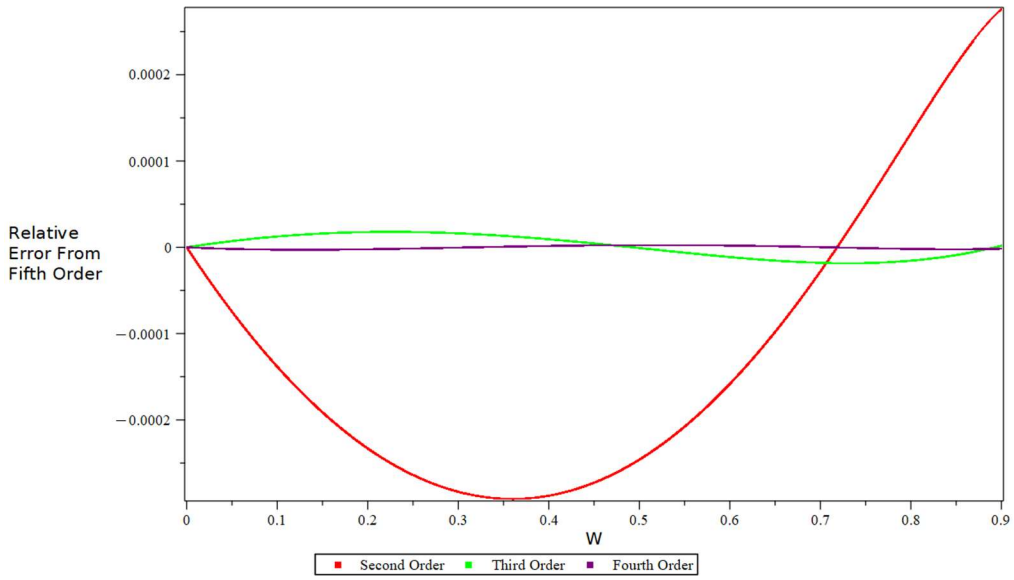

Fig. 38. Relative error of second to fourth order of the radial approximation term, A_r, to the 5th order approximation term.

The second order approximation improves on the first order approximation by 2 orders of magnitude, which reflects the same improvement in accuracy in the field approximation. The improvement from second to third order diminishes to approximately 1 order of magnitude. However, for the axial approximation, it is not as clear due to the subtraction of approximation terms A_z and B_z. Additionally, the coefficients on each ordered approximations are different and have a difference zeroth order term (either 1 or 3). These terms are not individually subtracted, but rather are part of the larger function, so

it makes it difficult to explicitly visualize the accuracy of the axial field independent of the axial field approximation. However, looking at A_z and B_z individually they follow the same behaviour with some minor scaling.

However, we can take advantage of the similarity of the additional higher order terms of the approximation. We've shown that the approximation terms for the radial and axial field components are all of a similar form, containing many of the same terms albeit with different coefficients.

$$A_R = \left[3 + A_{R1}\frac{W}{1-W} + A_{R2}\left(\frac{ln(1-W)}{W} + 1\right) + A_{R3}\ln\left(1-\mathrm{W}\right)\right] \qquad (67)$$

In Eq. 67 we see that the A_R terms all contain the same W for all orders of approximation at each point in space for each coil and the same is true for the A_z, B_z in the axial approximation. We also see that the second and third order approximation share the same ln(1-W) term. Then we only need to compute many of these terms once for both field directions, and we can reuse the same ln(1-W) term from the second order approximation for the third ordered term. A computationally efficient program would take advantage of this similarity to further reduce the computational cost for all orders of approximation. There, the 10x improvement in accuracy from the third ordered approximation comes at a nearly negligible computational cost.

4.1 First Order Helmholtz Approximation

We will explore the first order approximation for the Helmholtz coil system as described in Fig. 34 to see how the approximation accuracy evolves through to the second order approximation.

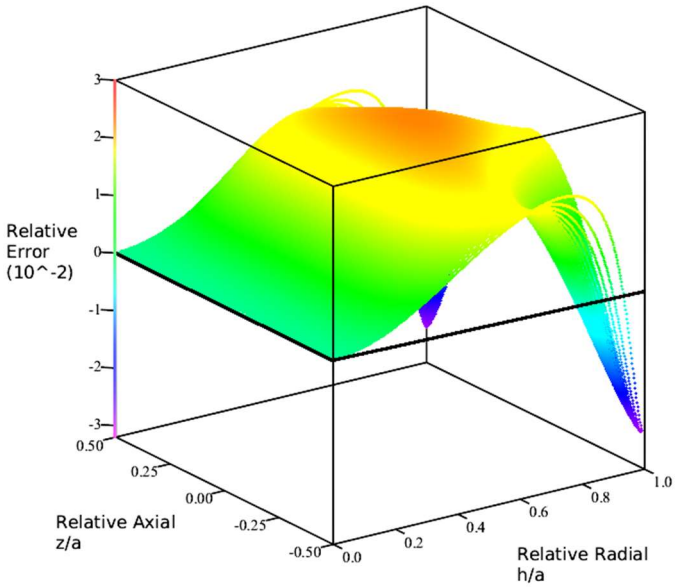

Fig. 39. First order Helmholtz coil radial field relative error.

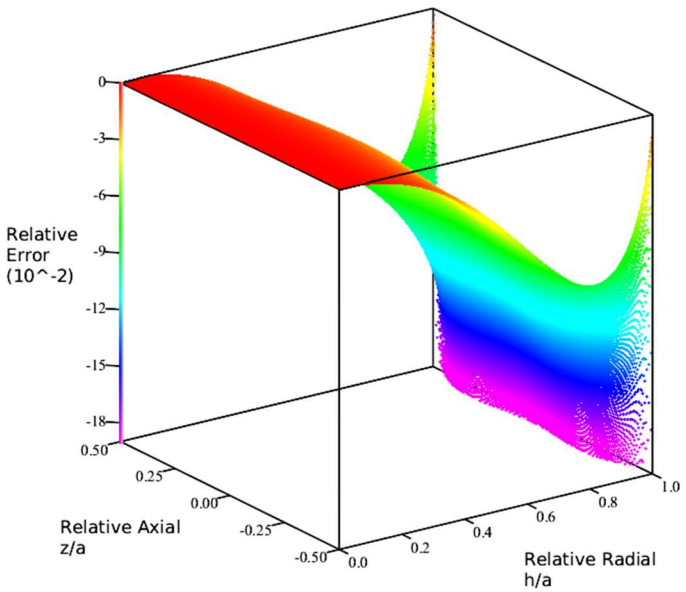

Fig. 40. First order Helmholtz coil axial field relative error.

We see similar behaviour as with a single current loop where the approximations are exactly correct along the coil axis and are accurate to 2 decimal places between the coils for both the radial field (Fig. 36) and the axial field (Fig. 37). As we approach either loop, $h = \pm\frac{a}{2}$ and $z = a$, the relative error begins to diverge as the field at the loop is singular. An important point here is that in chapter 2 we stated the first order axial loop approximation was not sufficiently accurate at the loop plane due to the lost degree of freedom. However, these Helmholtz relative error plots show that for a coil design, because always the contribution from one of the loops is away from the loop plane, the approximation's behaviour is much nicer. The maximum relative error is approximately 9% for h<0.9a, which is the same order of magnitude as the radial approximation. This makes it easy to both visualize how the field changes and perform quick calculations with the simple first order functions. Note also we are just looking within the loops, which is the important volume for coil design.

4.2 Second Order Helmholtz Approximation

The second order approximation provides additional degrees of freedom which forces the approximation to also be exact at W=1 for the radial component (see Fig. 38). For the axial component (Fig. 39), the additional degrees of freedom add an additional oscillation to the field in the loop plane, which flattens the maximum relative error. Most importantly, this leads to an improvement in accuracy by approximately two orders of magnitude, to the 0.02% range for radial and 0.2% range for the axial, and thus greatly improves the behaviour of the approximation was we approach the loop. The relative error begins to spike in both loop planes at approximately h=0.9 and then continues to diverge as we approach the loop. The additional degree of freedom also causes the relative error to oscillate above and below exactly correct. Whereas the first order approximations are nearly entirely above or below exactly correct.

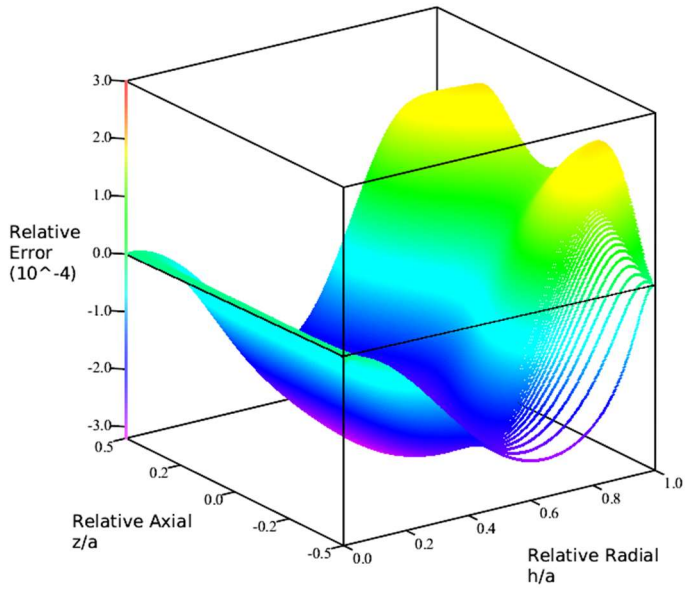

Fig. 41. Second order Helmholtz coil radial field relative error.

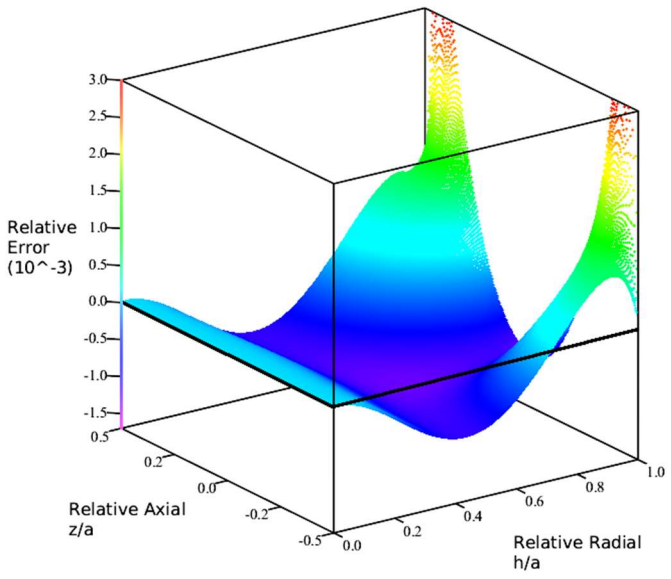

Fig. 42. Second order Helmholtz coil axial field relative error.

4.3 Third Order Helmholtz Approximation

The third order approximation adds additional degrees of freedom and for a single coil increase the accuracy by an order of magnitude. All with a nearly negligible computational cost as the additional term must already be calculated for the second order approximation. Visualizing the results below in Fig. 43 and Fig. 44 for the radial and axial approximations respectively.

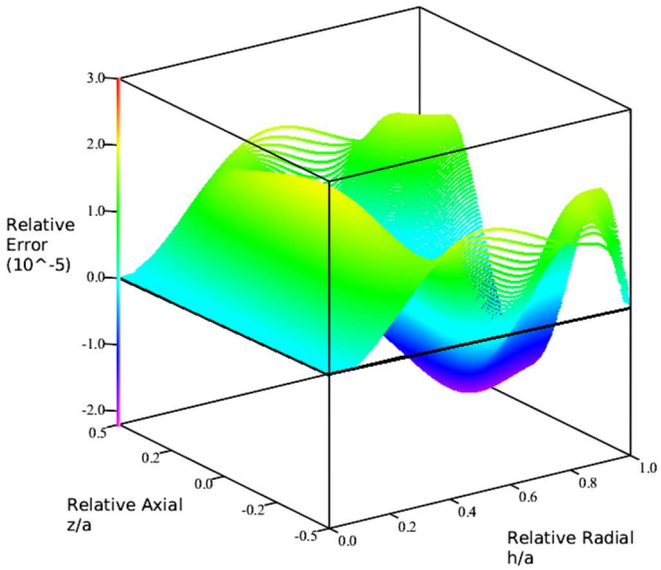

Fig. 43. Third order Helmholtz coil radial field relative error.

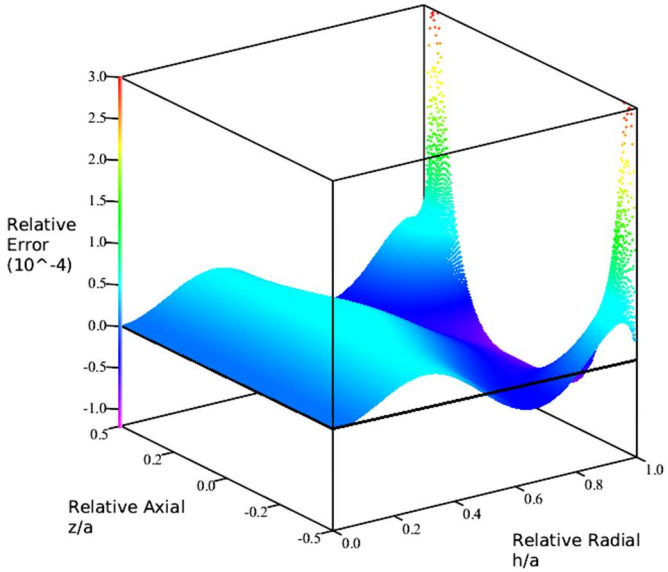

Fig. 44. Third order Helmholtz coil axial field relative error.

The increase in accuracy mirrors the magnitude increase for a single coil and we can see the added oscillation due to the additional degrees of freedom in both approximations. In summary, this seems to be the sweet spot for the approximation as we get a magnitude increase I the accuracy of the approximation for a nearly negligible computational cost. The third order approximation is accurate to nearly 5 and 4 significant figures for the radial and axial approximations respectively for the volume between the coils. Notably the axial approximation is accurate to 5 significant figures for $h<0.9a$, which is on the same order as the radial approximation.

4.4 Engineering Coil Design for Magnetic Field Uniformity

Determining the magnetic properties of a material or calibrating a magnetometer requires a magnetic field that is uniform to within a certain number of significant figures or relative uniformity. If an engineer needs to characterize the properties of a target material within a required accuracy, they must immerse the target material inside a Helmholtz coil where the field uniformity is within 1%. Therefore, there is some volume between the coils where the field deviates by less than 1% from the field along the coil axis. This engineering can use our approximations to determine the maximum volume between the pair of coils where the axial field varies within a fractional threshold. This volume is shown below in Fig. 45 and extends out radially and axially from the midpoint between the coils.

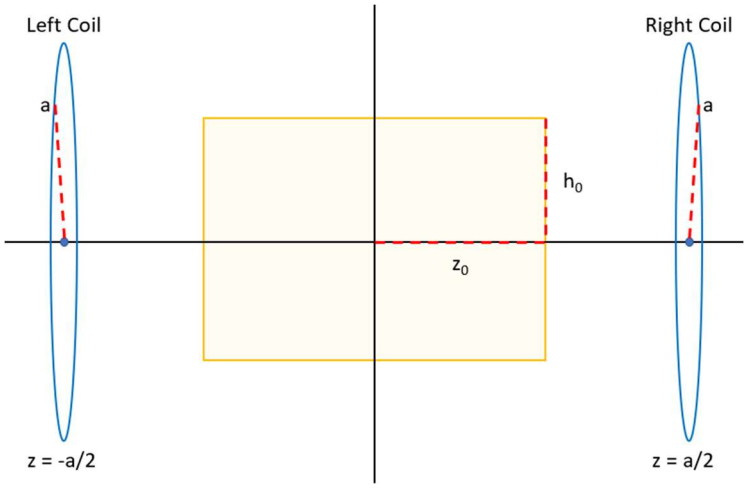

Fig. 45. Helmholtz coil system.

Determining this volume with the elliptical equations is computationally complex, but our approximations are simple enough that this can easily be done with a spreadsheet or pocket calculator. The threshold is the ratio of the axial field at a specific location to the axial field at the midpoint between the coils as shown below. We can solve for either the axial or radial distance first and then find the total enclosed volume with the first distance as a constraint.

These dimensions can quickly be found by searching first along the axis (z) or in the radial plane (h), starting at the midplane until the fractional field variation F at this new location is beyond the given threshold.

To describe this process, we will start by searching first in the radial plane and then along the axial direction at the specific radial component. Starting at the midpoint between the coils, we search radially outwards until the fractional field at the new location exceeds the user specified threshold T.

$$T \leq F = abs\left[\frac{B_z^{Helmholtz}(0,h)}{B_z^{Helmholtz}(0,0)}\right] \quad T \epsilon [0,1] \tag{68}$$

This gives us the radial location, $h = h_0$, where the field deviates beyond the required threshold. To find the second dimension, we follow the same process but by searching along the axial coordinate starting at h_0.

$$T \leq F = abs\left[\frac{B_z^{Helmholtz}(z,h_0)}{B_z^{Helmholtz}(0,0)}\right] \quad T \epsilon [0,1] \tag{69}$$

This provides the axial dimension, $z = z_0$, for our enclosed volume. As our simulations are setup, these dimensions are relative to the radial dimension of the coil. So that each returned dimension is some scaler multiplied by the coil radius. Referring to Fig. 45 we see that the total volume is described by the following equation which is cubic in terms of the radius of the coil.

$$Volume = \pi (2h_0)^2 (2z_0) \quad (70)$$

This simple algorithm allows engineers to quickly calculate what coil radius is required to produce a sufficiently uniform field for a known volume.

4.4 Summary

Our new approximations are exactly correct along the axis make on axis coil calculations exceptionally easy, even when applied to multiple coils such as in a Helmholtz coil. As we move off axis, we must calculate the approximation terms and the scaling factor individually for each coil, but the equations are still of lesser complexity than the elliptical equations. Our approximations remove the complexity of the elliptical integrals and are easy to solve with a handheld calculator or simple spreadsheet. Between the coils, the first order approximation is accurate to nearly 2 significant figures and may be suitable for many applications. This relative error is also comparable to the 1% maximum relative error using the series solution of nth order derivatives as discussed in the introduction [5]. However, the second order approximation's accuracy improves by 2 orders of magnitude to approximately 0.02%, which is significantly more accurate and computationally lower cost than the alternative method and is comparable to the 0.1% accuracy using Jackson's method [6]. However, these accuracies are quoted for a specific radius within the loop, h<= 0.7a and h<= 0.8a respectively. Whereas our solutions have comparable everywhere within the loop and notably, the second order approximations for the Helmholtz coils are exactly correct at the loop. Finally our 3rd order approximation improves the accuracy by another order of magnitude to nearly 5 significant figures for h<0.9 which is better than either alternative. Additionally, the 3rd order approximation has a nearly negligible increase in computational cost over second order as previously discussed and is the sweet spot for the trade off in accuracy and computational cost.

5. Conclusion

We have developed a series approximation for the radial and axial magnetic fields for a thin current loop. The accuracy of these approximations' ranges from 2 to 5 significant figures from first to fifth order approximations. These approximations are computationally simple and easy to visualize without intensive calculations when compared to their elliptical counterparts. Additionally, we have shown that these approximations are exactly correct along the loop axis, which is important as for many applications, engineers are mostly concerned with the field inside the loop (h<a).

Through my numerical simulations, we also have explored the previously unexplained singularities in the axial field relative error and demonstrated that this error arises due to the slight difference in the location where the axial field reverses polarity in the approximations and elliptical equations. Our work demonstrated and visualized the efficacy of these new approximations across all of 3D space. This thesis work enabled us to release the first publication of these equations at the end of my USRA to the Joint MMM Intermag 2021 conference in New Orleans (Jan. 2021) where it was also acceptable for a full journal publication in the IEEE Transactions on Magnetics [1, 8]. Our journal publication received its first citation in late 2022 where the author explored many magnetic current loop approximations, including ours where they confirmed the accuracy of our fifth order approximation [13].

We have also demonstrated that this approximation applies equally well for combinations of current loops in coil designs, as in the Helmholtz coil and evaluated the relative error of these approximations for the volume between the coils up to second order. We have also derived a simple algorithm using the approximations to calculate what coil radius is required to produce a sufficiently uniform field for a known volume.

In future work we recall that the second and third ordered approximations were derived by examining the factorial series for finite n. However, the fourth and fifth order were done adding additional corrective terms for the lowest n values, which does not provide the same improvement as examining the additional terms from the higher order Stirling's approximations. Adding additional corrective terms for by replacing Eq 35 with its series equivalent, if it is known and calculable, would likely lead to significant improvements in accuracy. This is equivalent to adding additional corrective terms from 3rd ordered and beyond terms for Stirling's approximation.

Importantly, these equations enable a trade-off between accuracy and computational cost for each order of approximation. Enabling designers to choose the computationally lowest cost approximation for their required accuracy. This also enables designers to first order approximations for quick initial designs and then expand to higher order for the refined design.

Due to the algebraic simplicity of these equations, there are future plans to explore previously computational complex problems. For example, it is clear that these approximations could be used to calculate the mutual inductance for two coils in any location. While existing literature solutions are tabulated for co-axial coils, solutions for other positions are more difficult. One would expect that only the 1st or 2nd order approximations are needed to achieve sufficiently high accuracy for this problem.

Similarly, we could apply these approximations to solve for the magnetic vector potential for a simple coil as well as complex systems containing multiple coils. Furthermore, as was noted in Chapman's MSc Thesis, the vector potential equation can be approximated in a similar way and have the advantage that would allow one to plot the magnetic field lines throughout the system [14].

One question of greater interest is to explore if we can use this same approximation method to generate solutions for the classic problem of solenoids (long helical coils) and pancake coils (wide, but flat donut coils), where useful equations for the general problems do not exist. In general, the simplicity of these approximations suggests that there are computationally simple approximations for many magnetic field systems and parameters.

References

[1] G. H. Chapman and D. E. Carleton, "Current Loop Off Axis field Approximations," in *Joint MMM Intermag*, New Orleans, 2022.

[2] W. R. Smythe, "Static and Dynamic Electricity (3rd Edition)," McGraw Hill, 1989, p. 290.

[3] M. Abramowitz and I. Stegun, “Handbook of Mathematical Functions”, 1970.

[4] W. R. Smythe, "Static and Dynamic Electricity (3rd Edition)," McGrawHill, 1989, p. 291.

[5] S. Karimian and G. Mehrshahi, "Accurate off-axis magnetic field calculation of axisymmetric cylindrical current distributions," *AIP Advances,* vol. 11, no. 095107, 2021.

[6] R. H. Jackson, "Off-axis expansion solution of Laplace's equation: Application to accurate and rapid calculation of coil magnetic fields," *IEEE Transactions on Electron Devices,* vol. 46, no. 5, pp. 1050-1062, 1999.

[7] "Ansys.com," [Online]. Available: www.ansys.com/products/electronics/ansys-maxwell. [Accessed 2022].

[8] G. H. Chapman, D. E. Carleton and D. G. Sahota, "Current Loop Off Axis Field Approximations with Excellent Accuracy and Low Computational Cost," *IEEE,* 22022.

[9] J. Robert A. Schill, "General Relation for the Vector Magnetic Field of a," *IEEE Transactions on Magnetics,* vol. 39, no. 2, 2003.

[10] J. C. Hastings, "Approximations for Digital Computers," *Princeton University Press,* 1955.

[11] D. W. Matson, "Magnetometer Calibration Services," *NIST,* 1995.

[12] Wikipedia, "wikipedia.org," [Online]. Available: https://en.wikipedia.org/wiki/Helmholtz_coil. [Accessed 2023].

[13] M. Ortner, P. Leitner and F. Slanovc, "Numerically Stable and Computationally Efficient Expression for the Magnetic Field of a Current Loop," *Magnetism,* vol. 3, no. 1, p. 11, 2022.

[14] G. H. Chapman, "Production and Testing of Pico ohm Resistance Joints," *MSc thesis, Queen’s University,* 1975.

Appendix A.

A.1 Code Repository

https://drive.google.com/drive/folders/1eeJY-7pGVOc0n6z5p94DD3CmOr62_2aK?usp=sharing